Electronic Supplementary Material (ESI) for Soft Matter.

- Electronic Supplementary Information -

Multi-Energy Dissipation Mechanisms in Supramolecular Hydrogels with Fast and Slow Relaxation Modes

Subaru Konishi,[a] Junsu Park,[a,c] Osamu Urakawa,[a] Motofumi Osaki,[a,c] Hiroyasu Yamaguchi,[a,c,d] Akira Harada,[e] Tadashi Inoue,[a,c] Go Matsuba,*[f] and Yoshinori Takashima*[a,b,c,d]

[a] Department of Macromolecular Science, Graduate School of Science, Osaka University, 1-1 Machikaneyama, Toyonaka, Osaka 560-0043 Japan.

[b] Institute for Advanced Co-Creation Studies, Osaka University, 2-1 Yamada-oka, Suita, Osaka 565-0871 Japan.

[c] Forefront Research Center, Osaka University, 1-1 Machikaneyama, Toyonaka, Osaka 560-0043 Japan.

[d] SANKEN (The Institute of Scientific and Industrial Research), Osaka University, 8-1 Mihogaoka, Ibaraki, Osaka 567-0047 Japan.

[e] Institute for Open and Transdisciplinary Research Initiatives, Osaka University, 2-1 Yamada-oka, Suita, Osaka 565-0871 Japan.

[f] Graduate School of Organic Material Engineering, Yamagata University, 4-3-16 Jonan, Yonezawa, Yamagata 992-8510, Japan.

E-mail: gmatsuba@yz.yamagata-u.ac.jp

takasima@chem.sci.osaka-u.ac.jp.

Content

1. Experimental details

Materials

Acrylamide (AAm) and *N*-(hydroxymethyl)acrylamide were purchased from Wako Pure Chemical Industries, Ltd. α-Cyclodextrin (αCD) was obtained from Junsei Chemical Co. Ltd. Acetone, methanol, diethyl ether, ethyl acetate, acrylic acid, hydrochloric acid, sodium hydroxide, sodium sulfate, *p*-toluenesulfonic acid monohydrate, potassium chloride (KCl), potassium peroxodisulfate (KPS), *N*,*N*,*N*′,*N*′–tetramethylethylenediamine (TEMED), *N*,*N*′–methylenebis(acrylamide) (MBAAm), 1-methylimidazole and pyridine were purchased from Nacalai Tesque Inc. Dimethyl sulfoxide-d_6 (DMSO-d_6) was obtained from Merck & Co., Inc. Chloroform-*d* ($CDCl_3$) and deuterium oxide (D_2O) were obtained from EURISO-TOP. 4,4'-Bipyridyl and trimethylamine (in acetonitrile) were purchased from Tokyo Kasei. Water used for preparing aqueous solutions was purified with a Millipore Elix 5 system. Other reagents were used without further purification. Acrylamido-methyl ether-modified αCD (αCDAAmMe), 3-(11-acryloyloxyundecyl)-1-methyl-imidazolium bromide (ImC11 monomer), 1-(11-acryloyloxyundecyl)-pyridinium bromide (PyC11 monomer), 4-(11-acryloyloxyundecyl)-4'-(methyl)-bipyridinium dichloride (VC11 monomer), and 11-acryloyloxyundecyl trimethylammonium bromide (TMAmC11 monomer) were prepared according to our previous reports.[1–4]

Measurements

^{1}H and ^{13}C nuclear magnetic resonance (NMR) spectroscopy: ^{1}H and ^{13}C NMR spectra were recorded with a JEOL JNM–ECA 400 NMR spectrometer (400 MHz) and a JEOL JNM–ECA 500 NMR spectrometer (500 MHz). Solid-state ^{1}H field gradient magic angle spinning (FG-MAS) NMR spectra were recorded with a JEOL JNM–ECA 400 NMR spectrometer (400 MHz, with a sample spinning rate of 7 kHz). 2-Dimensional ^{1}H-^{1}H Nuclear Overhauser Effect spectroscopy (2D NOESY) NMR spectra were obtained at 600 MHz with an Agilent VNS600 NMR spectrometer at 25 °C. The mixing time for 2D NOESY NMR was set to 500 ms. All chemical shifts were referenced to residual solvent peaks as internal standards (for ^{1}H NMR: δ = 0 ppm for tetramethylsilane (TMS), 2.49 ppm for DMSO–d_6, 4.79 ppm for D_2O, and 7.26 ppm for $CDCl_3$; ^{13}C NMR: δ = 0 ppm for TMS, 39.5 ppm for DMSO–d_6, and 77.0 ppm for $CDCl_3$).

Fourier transform infrared (FT-IR) spectroscopy: FT-IR spectra were acquired at room temperature using a JASCO FT/IR–6100 spectrometer in the wavenumber range 600 to 4000 cm^{-1} via the attenuated total reflection (ATR) method using a ZnSe prism.

Tensile tests: Tensile tests and cyclic tensile tests were performed on a universal testing machine [Autograph AG-X plus (Shimadzu Co.)] equipped with a 20 N load cell and 1 N clip grips. The hydrogels were prepared using a type 4 dumbbell-shaped Teflon mold by following the ISO 37 (JIS K6251) standard. For tensile tests, the hydrogels were stretched at a tensile rate of 1 mm/s at approximately 25 °C. Based on the stress–strain curves, fracture strengths and strains were defined as the maximum stress and strain before stress decreased. Toughness was calculated from the integral of the stress–strain curve, and the fracture strain was set as the upper limit of the integral. Young's modulus was calculated from the initial slope of the stress–strain curve within a strain range between 3%–8%. The error bars (standard deviation) for toughness and Young's modulus

were calculated from more than three experiments. For cyclic tensile tests, the hydrogels were stretched and recovered at approximately 25 °C with a tensile rate of 1 mm/s without intervals. Then, the maximum strains were set to 16%, 32%, 48%, 64% and 80% of the fracture strain of each hydrogel. The hysteresis ratio at each cycle was calculated using equation (1). The error bars for the hysteresis areas and hysteresis ratios were calculated from more than three experiments.

$$\text{Hysteresis ratio (\%)} = \frac{\text{Hysteresis area}}{\text{Supplied work under loading}} \times 100 \quad (1)$$

Rheological measurements: Dynamic viscoelasticity and stress-relaxation properties were measured using an Anton Paar MCR302 rheometer with a parallel-plate fixture (8 mm in diameter). An angular frequency (ω) sweep from 0.1 to 100 rad/s was performed using a parallel-plate fixture 8 mm in diameter over a temperature range of 0–45 °C. Stress-relaxation tests were performed at 25 °C. The oscillatory shear strain (γ) induced in both ω sweep and stress-relaxation tests was within the range of linear viscoelasticity. Details of the analysis method are described below.

Small-angle X-ray scattering (SAXS) measurements: The internal structures of the hydrogels under stretching were analyzed by SAXS with a tensile device at the BL40B2 beamline of SPring-8, Nishiharima, Japan. The wavelength of the incident X-ray beams was 0.10 nm. The sample-to-detector lengths were 2000 and 2282 mm. Type 4 dumbbell-shaped hydrogels with thicknesses of approximately 1 or 2.4 mm were prepared and cut to 15 mm lengths to fit the tensile device. They were stretched at room temperature with a tensile rate of 0.63 mm/s to adjust the initial strain rates to values similar to those of the tensile tests. When the strain (ε_c) of the hydrogel reached 0%, 50%, 100%, 200%, 300% and 400%, the strain was fixed for 90~120 s, and then the SAXS profiles were recorded. The obtained 1D SAXS profiles were converted into absolute intensity (I_{abs}) with equation (2) to eliminate the effects of exposure time (t_e), transmittance (T) and thickness of gels (Z). In concrete terms, the 1D SAXS profiles of the hydrogels and background were normalized

with t_e, T and Z. Then, assuming affine deformation of the hydrogels, the thickness at each ε_c was theoretically corrected by the initial thickness (Z_0) and ε_c with equation (3). Note that the detection efficiency of the measuring device was not taken into account.

$$Absolute\ intensity\ (I_{\mathrm{abs}}) = \frac{Obtained\ profile}{t_e T Z} - \frac{background}{t_e Z} \tag{2}$$

$$Z = \frac{Z_0}{\sqrt{1+\varepsilon_C}} \tag{3}$$

2. Preparation of the supramolecular hydrogels

Preparation of the αCD-ImC11-PyC11 (2, 1, 1) hydrogel

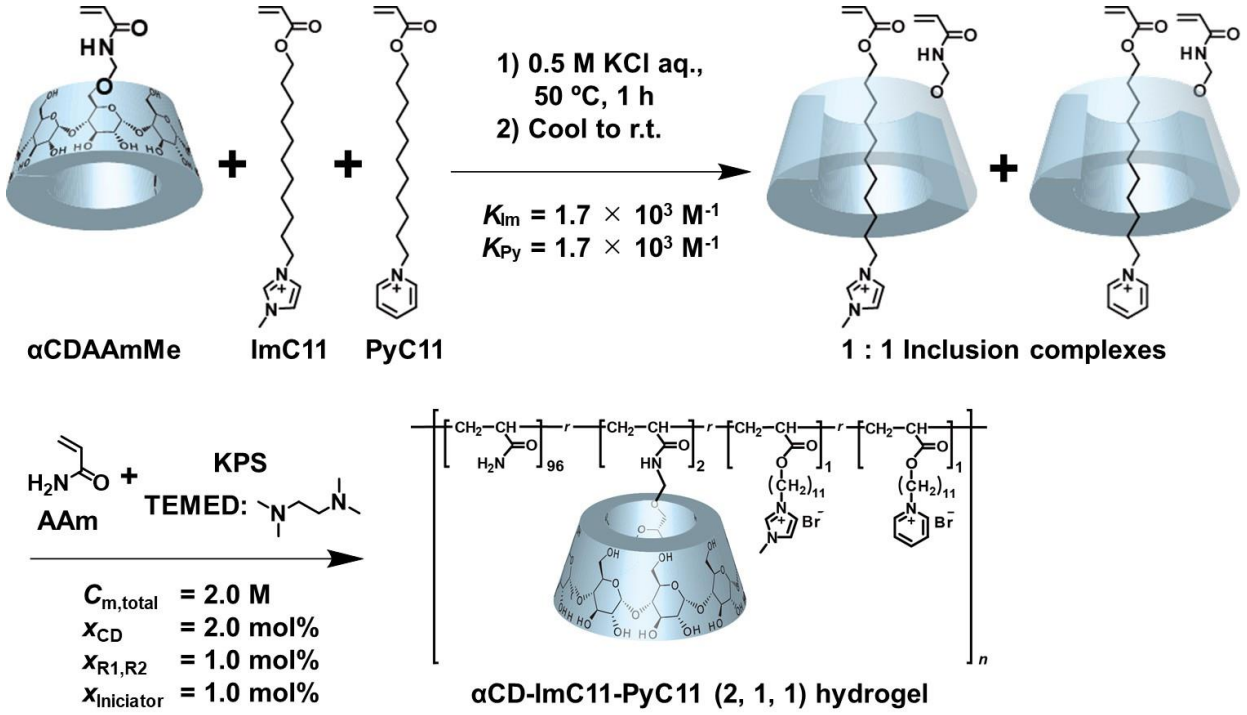

Scheme S1. Preparation of the αCD-ImC11-PyC11 (2, 1, 1) hydrogel.

αCDAAmMe (84 mg, 0.080 mmol), ImC11 (16 mg, 0.040 mmol) and PyC11 (15 mg, 0.040 mmol) were mixed in 0.5 M KCl aq. for an hour at 50 °C under sonication to form the host-guest inclusion complex. The inclusion complexes of αCDAAmMe with ImC11 and PyC11 were copolymerized with AAm (the main chain monomer, 273 mg, 3.84 mmol) by using a redox initiator system (11 mg (0.040 mmol) of KPS and 4.6 mg (0.040 mmol) of TEMED) in a mold at room temperature. The solution gelated within 5 minutes to give a self-standing hydrogel. The hydrogels were characterized by FG-MAS NMR, 2D NMR and IR spectroscopy (**Figures S1, S2, and S8**). The amounts of reagents and the solvent used are summarized in **Table S1**.

Other αCD-R_1-R_2 (2, 1, 1) and αCD-R (2, 2) hydrogels were prepared in the same way, and the reagents and solvent used are summarized in **Tables S2–S15**. In the case of the αCD-PyC11-MBAAm (1, 1, *x*) hydrogels, MBAAm was added to the reaction system simultaneously with AAm.

Table S1. Amounts of reagents and solvents used in the preparation of the αCD-ImC11-PyC11 (2, 1, 1) hydrogel.

	KCl aq. /mL	AAm /mg	αCDAAmMe /mg	ImC11 /mg	PyC11 /mg	KPS /mg	TEMED /μL
αCD-ImC11-PyC11 (2, 1, 1) hydrogel	2.0	273	84.5	15.5	15.4	10.8	6.0

Table S2. Amounts of reagents and solvents used in the preparation of the αCD-ImC11-VC11 (2, 1, 1) hydrogel.

	KCl aq. /mL	AAm /mg	αCDAAmMe /mg	ImC11 /mg	VC11 /mg	KPS /mg	TEMED /μL
αCD-ImC11-VC11 (2, 1, 1) hydrogel	2.0	273	84.5	15.5	18.7	10.8	6.0

Table S3. Amounts of reagents and solvents used in the preparation of the αCD-ImC11-TMAmC11 (2, 1, 1) hydrogel.

	KCl aq. /mL	AAm /mg	αCDAAmMe /mg	ImC11 /mg	TMAmC11 /mg	KPS /mg	TEMED /μL
αCD-ImC11-TMAmC11 (2, 1, 1) hydrogel	2.0	273	84.5	15.5	14.6	10.8	6.0

Table S4. Amounts of reagents and solvents used in the preparation of the αCD-PyC11-VC11 (2, 1, 1) hydrogel.

	KCl aq. /mL	AAm /mg	αCDAAmMe /mg	PyC11 /mg	VC11 /mg	KPS /mg	TEMED /μL
αCD-PyC11-VC11 (2, 1, 1) hydrogel	2.0	273	84.5	15.4	18.7	10.8	6.0

Table S5. Amounts of reagents and solvents used in the preparation of the αCD-PyC11-TMAmC11 (2, 1, 1) hydrogel.

	KCl aq. /mL	AAm /mg	αCDAAmMe /mg	PyC11 /mg	TMAmC11 /mg	KPS /mg	TEMED /μL
αCD-PyC11-TMAmC11 (2, 1, 1) hydrogel	2.0	273	84.5	15.4	14.6	10.8	6.0

Table S6. Amounts of reagents and solvents used in the preparation of the αCD-VC11-TMAmC11 (2, 1, 1) hydrogel.

	KCl aq. /mL	AAm /mg	αCDAAmMe /mg	VC11 /mg	TMAmC11 /mg	KPS /mg	TEMED /μL
αCD-VC11-TMAmC11 (2, 1, 1) hydrogel	2.0	273	84.5	18.7	14.6	10.8	6.0

Table S7. Amounts of reagents and solvents used in the preparation of the αCD-ImC11 (2, 2) hydrogel.

	KCl aq. /mL	AAm /mg	αCDAAmMe /mg	ImC11 /mg	KPS /mg	TEMED /μL
αCD-ImC11 (2, 2) hydrogel	2.0	273	84.5	31.0	10.8	6.0

Table S8. Amounts of reagents and solvents used in the preparation of the αCD-PyC11 (2, 2) hydrogel.

	KCl aq. /mL	AAm /mg	αCDAAmMe /mg	PyC11 /mg	KPS /mg	TEMED /μL
αCD-PyC11 (2, 2) hydrogel	2.0	273	84.5	30.8	10.8	6.0

Table S9. Amounts of reagents and solvents used in the preparation of the αCD-VC11 (2, 2) hydrogel.

	KCl aq. /mL	AAm /mg	αCDAAmMe /mg	VC11 /mg	KPS /mg	TEMED /μL
αCD-VC11 (2, 2) hydrogel	2.0	273	84.5	37.4	10.8	6.0

Table S10. Amounts of reagents and solvents used in the preparation of the αCD-TMAmC11 (2, 2) hydrogel.

	KCl aq. /mL	AAm /mg	αCDAAmMe /mg	TMAmC11 /mg	KPS /mg	TEMED /μL
αCD-TMAmC11 (2, 2) hydrogel	2.0	273	84.5	29.1	10.8	6.0

Table S11. Amounts of reagents and solvents used in the preparation of the αCD-PyC11-MBAAm (1, 1, 0.5) hydrogel.

	KCl aq. /mL	AAm /mg	αCDAAmMe /mg	PyC11 /mg	MBAAm /mg	KPS /mg	TEMED /μL
αCD-PyC11-MBAAm (1, 1, 0.5) hydrogel	2.0	277	42.2	15.4	3.1	10.8	6.0

Table S12. Amounts of reagents and solvents used in the preparation of the αCD-PyC11-MBAAm (1, 1, 1) hydrogel.

	KCl aq. /mL	AAm /mg	αCDAAmMe /mg	PyC11 /mg	MBAAm /mg	KPS /mg	TEMED /μL
αCD-PyC11-MBAAm (1, 1, 1) hydrogel	2.0	276	42.2	15.4	6.2	10.8	6.0

Table S13. Amounts of reagents and solvents used in the preparation of the αCD-PyC11-VC11-TMAmC11 (2, 0.67, 0.67, 0.67) hydrogel.

	KCl aq. /mL	AAm /mg	αCDAAmMe /mg	PyC11 /mg	VC11 /mg	TAMmC11 /mg	KPS /mg	TEMED /μL
αCD-PyC11-VC11-TMAmC11 (2, 0.67, 0.67, 0.67) hydrogel	1.2	164	50.7	6.2	7.5	5.9	6.5	3.6

Table S14. Amounts of reagents and solvents used in the preparation of the αCD-PyC11-VC11-TMAmC11 (3, 1, 1, 1) hydrogel.

	KCl aq. /mL	AAm /mg	αCDAAmMe /mg	PyC11 /mg	VC11 /mg	TAMmC11 /mg	KPS /mg	TEMED /μL
αCD-PyC11-VC11-TMAmC11 (3, 1, 1, 1) hydrogel	1.2	160	76.0	9.2	11.2	8.7	6.5	3.6

Table S15. Amounts of reagents and solvents used in the preparation of the αCD-PyC11-VC11-TMAmC11 (2, 1, 0.5, 0.5) hydrogel.

	KCl aq. /mL	AAm /mg	αCDAAmMe /mg	PyC11 /mg	VC11 /mg	TAMmC11 /mg	KPS /mg	TEMED /μL
αCD-PyC11-VC11-TMAmC11 (2, 1, 0.5, 0.5) hydrogel	1.2	164	50.7	9.2	5.6	4.4	6.5	3.6

3. Characterization of the supramolecular hydrogels by IR and NMR spectroscopy

FT-IR spectra

Figure S1 shows the FT-IR difference spectra of the αCD-R_1-R_2 (2, 1, 1) hydrogels at room temperature in the attenuated total reflection (ATR) method using a ZnSe prism. The as-prepared αCD-R_1-R_2 hydrogels were freeze-dried to eliminate water. The freeze-dried gels were swollen with D_2O and analyzed by FT-IR spectroscopy. Difference spectra were calculated by subtracting that of D_2O from those of the αCD-R_1-R_2 hydrogels. Then, the spectrum of D_2O was multiplied by a coefficient to adjust the subtraction at approximately 1200 or 2500 cm^{-1}. The absorbance of the difference spectra was very weak, approximately 2~10%. These are reasonable values because the water contents of the swollen hydrogels should be more than 90 wt%. The observed peaks in the difference spectra of the αCD-R_1-R_2 hydrogels mainly reflected the poly(acrylamide) main chain.

Analyses of the αCD-R (2, 2) hydrogels by FT-IR spectroscopy were reported in our previous work.[3]

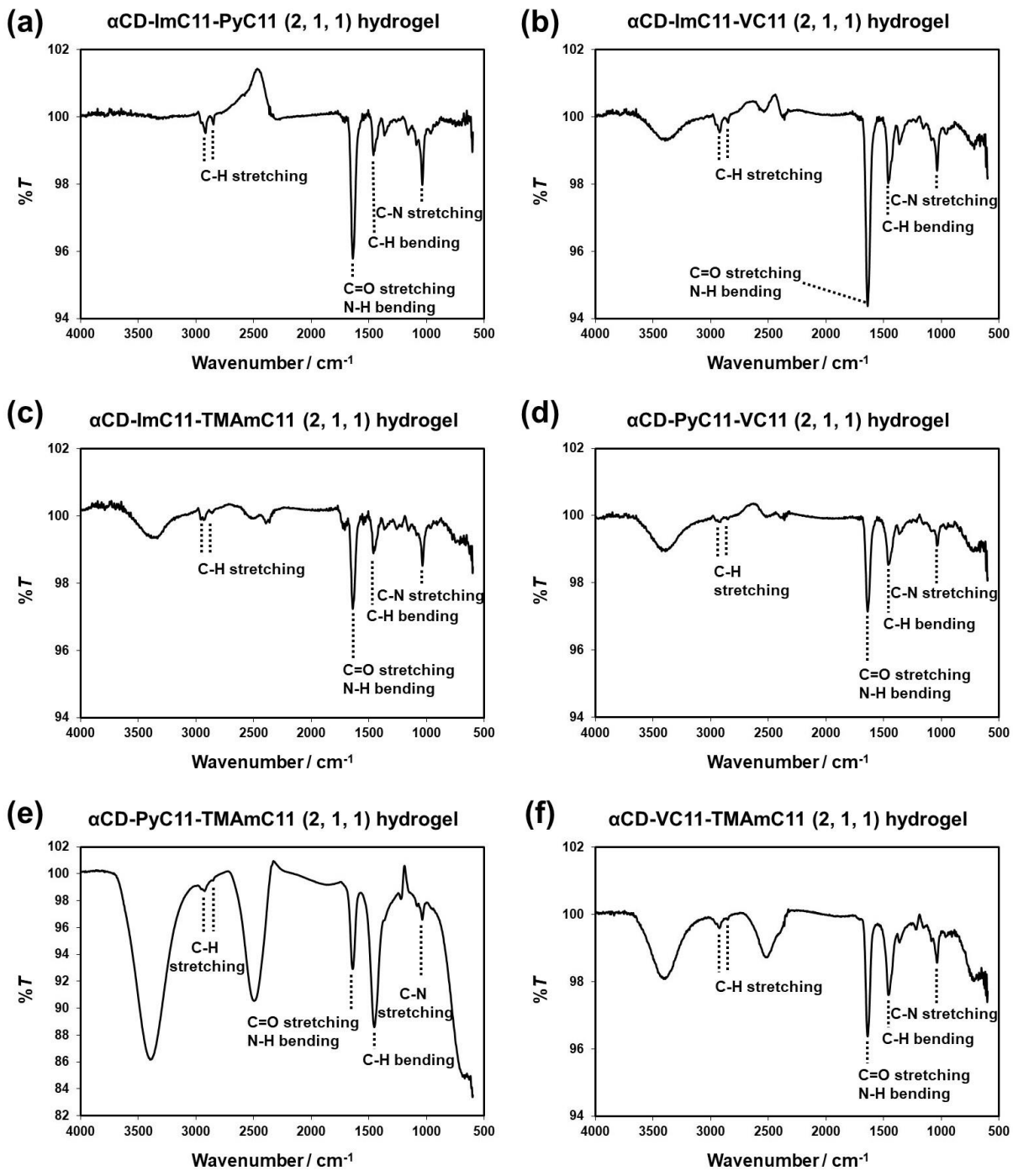

Figure S1. FT-IR difference spectra of **(a)** αCD-ImC11-PyC11 (2, 1, 1), **(b)** αCD-ImC11-VC11 (2, 1, 1), **(c)** αCD-ImC11-TMAmC11 (2, 1, 1), **(d)** αCD-PyC11-VC11 (2, 1, 1), **(e)** αCD-PyC11-TMAmC11 (2, 1, 1), and **(f)** αCD-VC11-TMAmC11 (2, 1, 1) hydrogels immersed in D_2O.

FG-MAS NMR spectra

The as-prepared αCD-R_1-R_2 (2, 1, 1) hydrogels were freeze-dried, immersed in D_2O, and analyzed by FG-MAS spectroscopy (**Figures S2–S7**). The αCD-R (2, 2) hydrogels were analyzed in our previous work.[3]

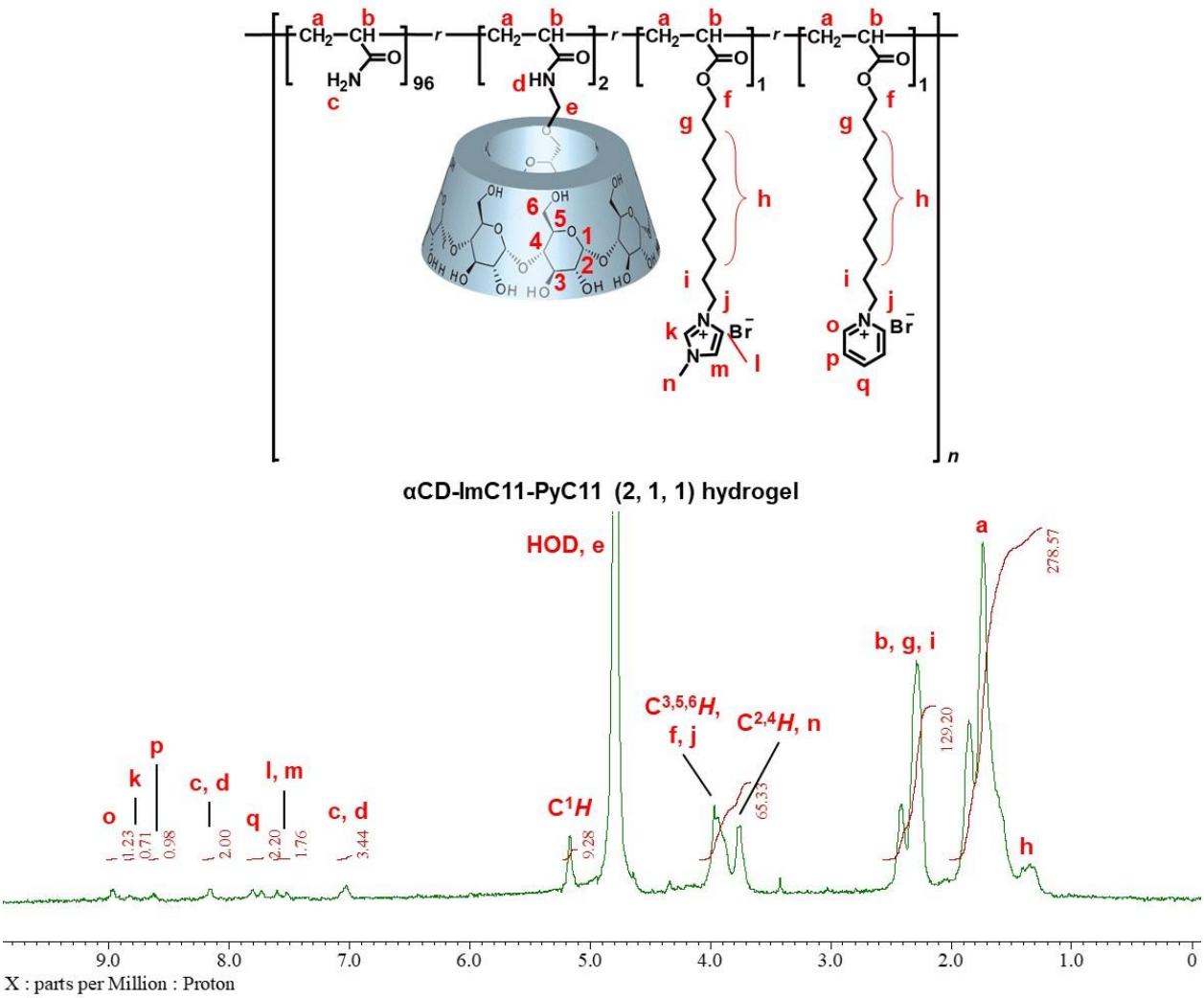

Figure S2. 400 MHz ^{1}H FG-MAS NMR spectrum of the αCD-ImC11-PyC11 (2, 1, 1) hydrogel immersed in D_2O at 25 °C. The frequency of the magic angle spinning was 7 kHz.

Amount of each residue

In the preparation: [AAm]/[αCD]/[ImC11]/[PyC11] = 96.0/2.0/1.0/1.0.
Calculated from the spectrum: [AAm]/[αCD]/[ImC11]/[PyC11] = 97.2/1.2/0.8/0.8.

^{1}H NMR: δ = 8.96, 8.83, 8.63, 8.16, 7.76, 7.56, 7.03, 5.17, 4.04–3.82, 3.82–3.68, 2.58–2.10, 2.00–1.46, 1.46–1.20.

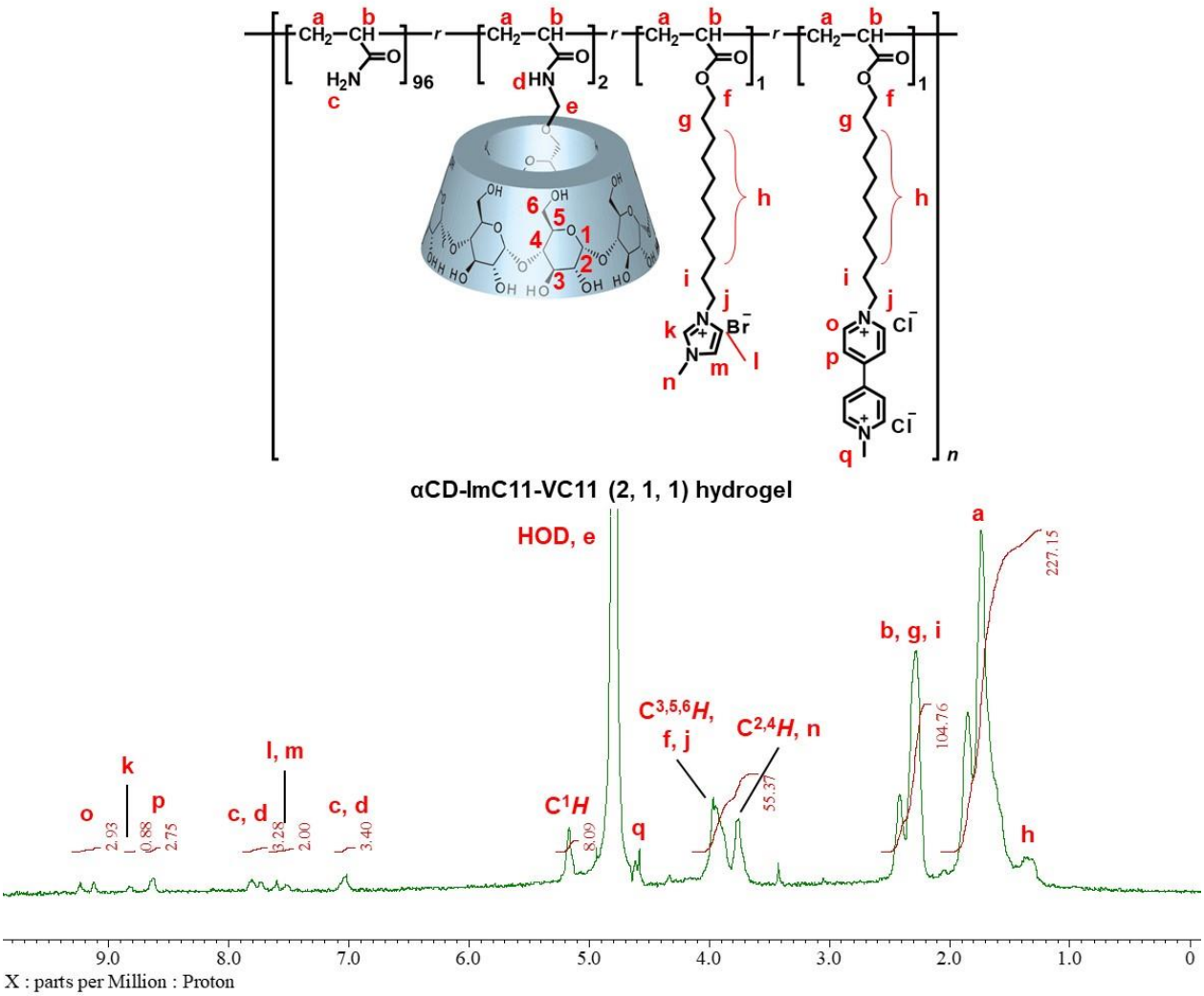

Figure S3. 400 MHz ^{1}H FG-MAS NMR spectrum of the αCD-ImC11-VC11 (2, 1, 1) hydrogel immersed in D_2O at 25 °C. The frequency of the magic angle spinning was 7 kHz.

Amount of each residue

In the preparation: [AAm]/[αCD]/[ImC11]/[VC11] = 96.0/2.0/1.0/1.0.
Calculated from the spectrum: [AAm]/[αCD]/[ImC11]/[VC11] = 96.9/1.4/1.0/0.7.

^{1}H NMR: δ = 9.18, 8.83, 8.64, 7.77, 7.60, 7.52, 7.02, 5.17, 4.58, 4.08–3.82, 3.82–3.66, 2.54–2.16, 2.00–1.46, 1.46–1.20.

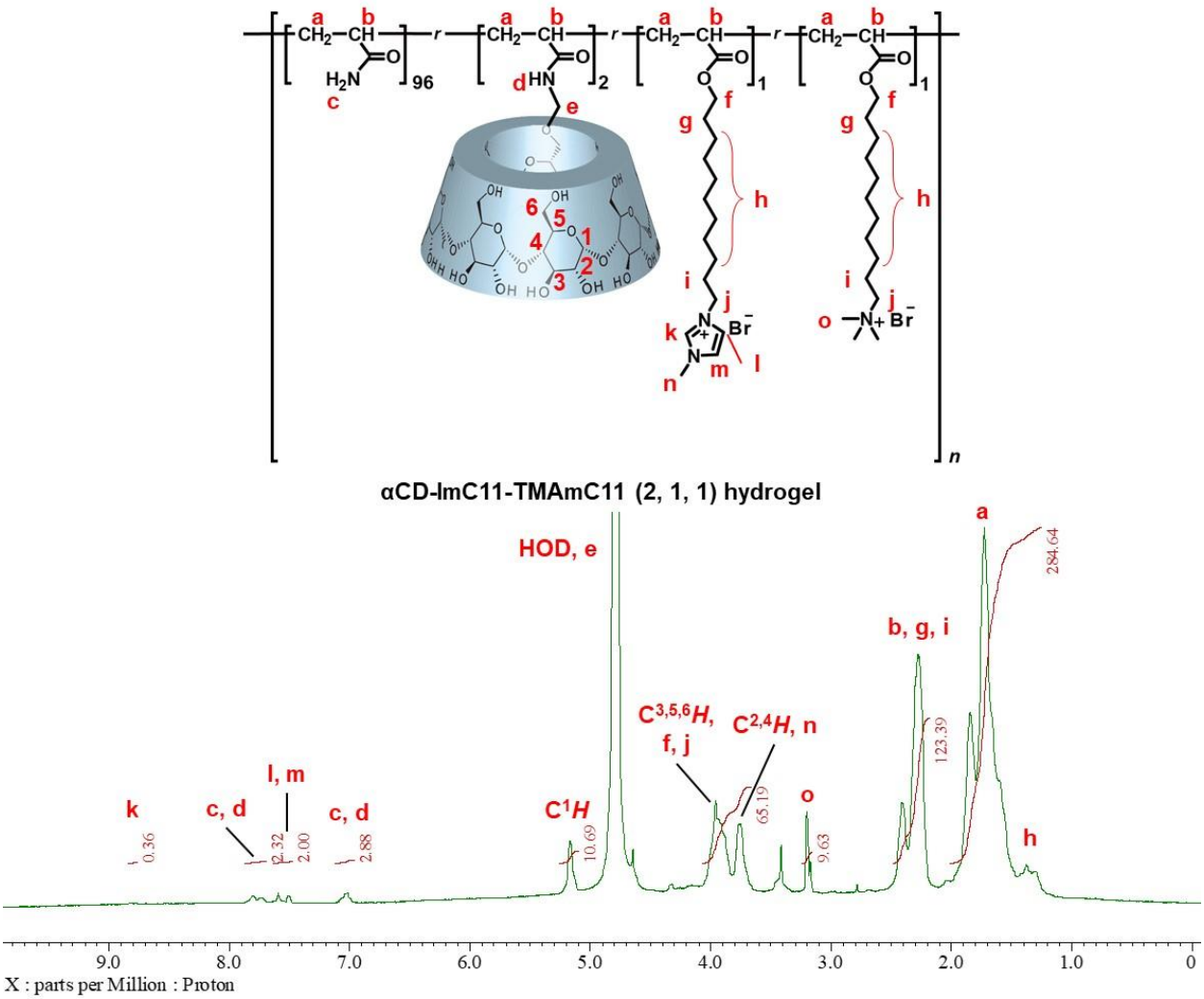

Figure S4. 400 MHz ^{1}H FG-MAS NMR spectrum of the αCD-ImC11-TMAmC11 (2, 1, 1) hydrogel immersed in D_2O at 25 °C. The frequency of the magic angle spinning was 7 kHz.

Amount of each residue

In the preparation: [AAm]/[αCD]/[ImC11]/[TMAmC11] = 96.0/2.0/1.0/1.0.
Calculated from the spectrum: [AAm]/[αCD]/[ImC11]/[TMAmC11] = 96.9/1.4/0.8/0.9.

^{1}H NMR: δ = 8.82, 7.77, 7.59, 7.50, 7.02, 5.17, 4.08–3.83, 3.83–3.62, 3.20, 2.51–2.16, 2.00–1.46, 1.46–1.18.

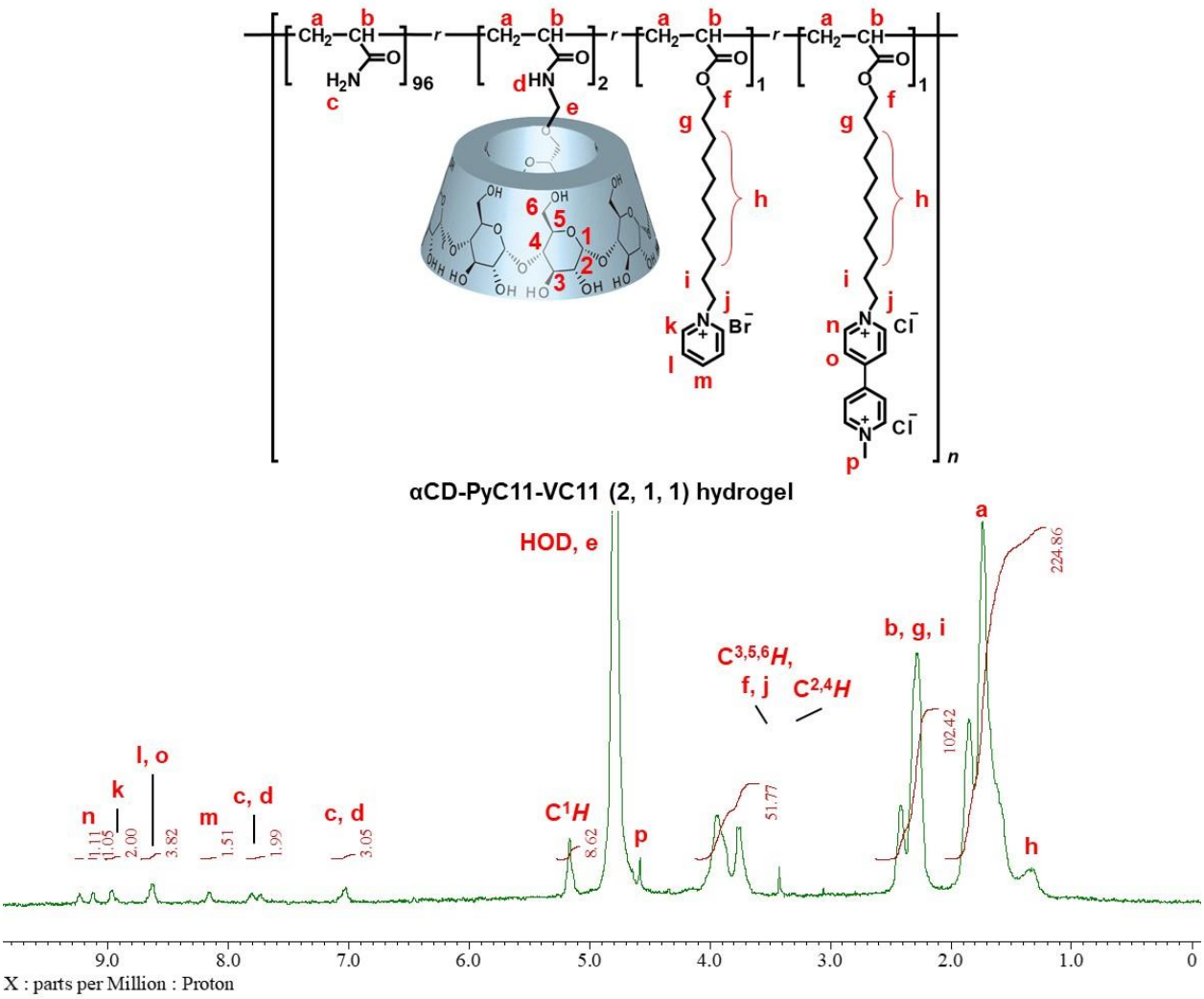

Figure S5. 400 MHz ^{1}H FG-MAS NMR spectrum of the αCD-PyC11-VC11 (2, 1, 1) hydrogel immersed in D_2O at 25 °C. The frequency of the magic angle spinning was 7 kHz.

Amount of each residue

In the preparation: [AAm]/[αCD]/[PyC11]/[VC11] = 96.0/2.0/1.0/1.0.
Calculated from the spectrum: [AAm]/[αCD]/[PyC11]/[VC11] = 96.9/1.5/1.0/0.6.

^{1}H NMR: δ = 9.18, 8.96, 8.64, 8.16, 7.77, 7.02, 5.17, 4.58, 4.10–3.82, 3.82–3.64, 2.52–2.16, 2.00–1.45, 1.45–1.20.

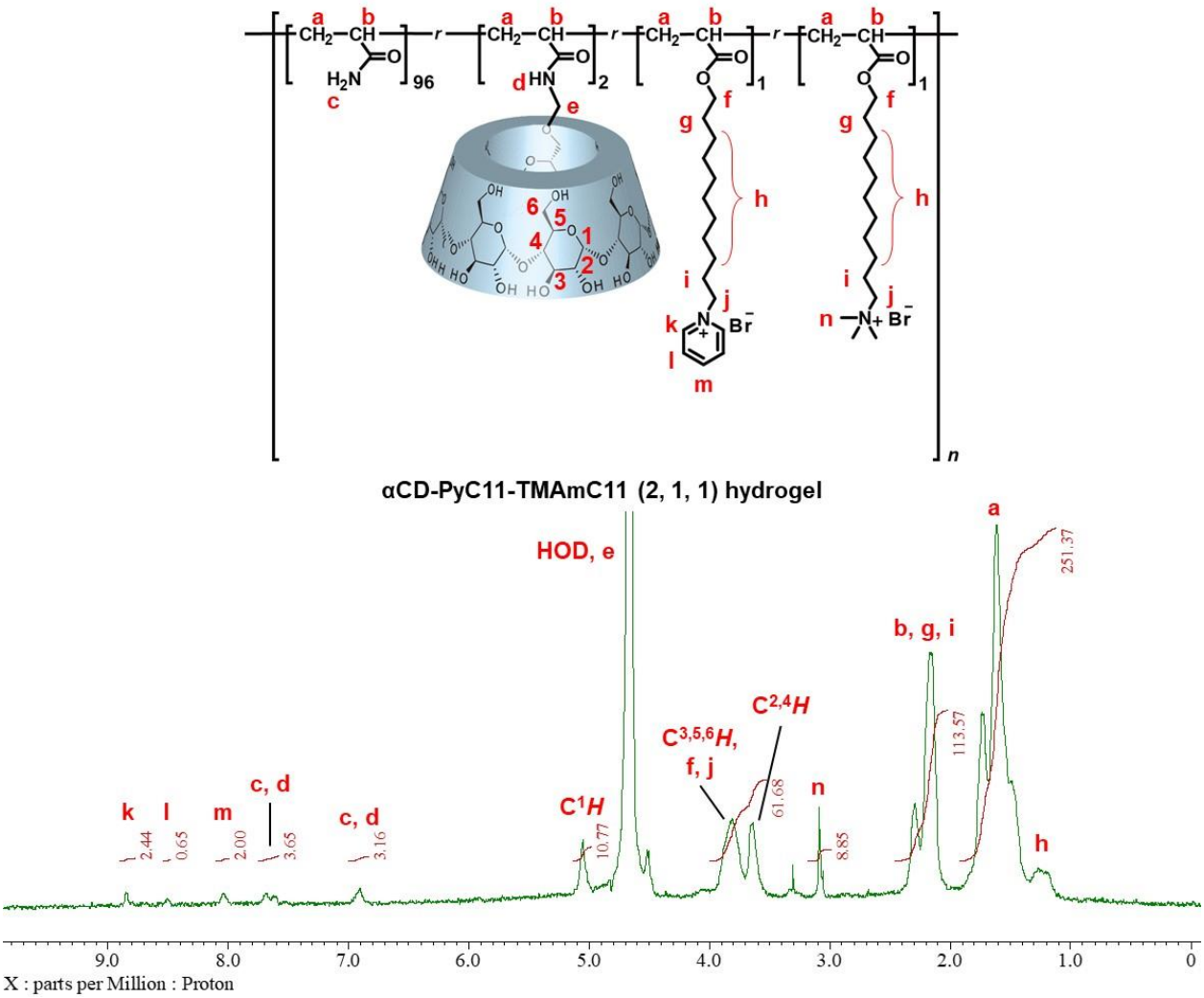

Figure S6. 400 MHz ^{1}H FG-MAS NMR spectrum of the αCD-PyC11-TMAmC11 (2, 1, 1) hydrogel immersed in D_2O at 25 °C. The frequency of the magic angle spinning was 7 kHz.

Amount of each residue

In the preparation: [AAm]/[αCD]/[PyC11]/[TMAmC11] = 96.0/2.0/1.0/1.0.
Calculated from the spectrum: [AAm]/[αCD]/[PyC11]/[TMAmC11] = 96.6/1.6/0.9/0.9.

^{1}H NMR: δ = 8.85, 8.50, 8.04, 7.65, 6.91, 5.05, 4.00–3.69, 3.69–3.52, 3.09, 2.44–2.02, 1.92–1.36, 1.36–1.06.

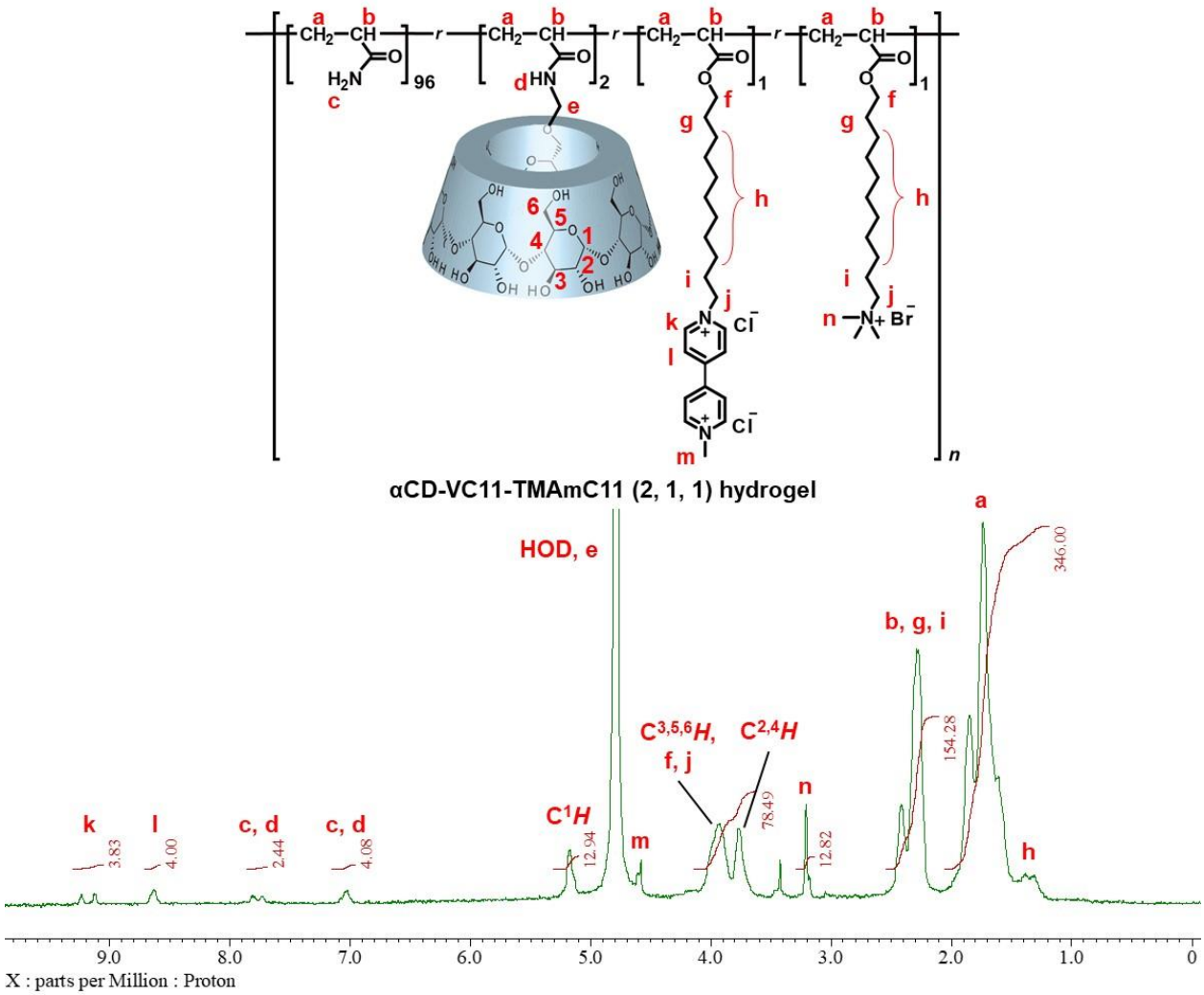

Figure S7. 400 MHz ^{1}H FG-MAS NMR spectrum of the αCD-VC11-TMAmC11 (2, 1, 1) hydrogel immersed in D_2O at 25 °C. The frequency of the magic angle spinning was 7 kHz.

Amount of each residue

In the preparation: [AAm]/[αCD]/[VC11]/[TMAmC11] = 96.0/2.0/1.0/1.0.
Calculated from the spectrum: [AAm]/[αCD]/[VC11]/[TMAmC11] = 97.0/1.4/0.7/0.9.

^{1}H NMR: δ = 9.18, 8.64, 7.77, 7.03, 5.18, 4.58, 4.12–3.83, 3.83–3.62, 3.21, 2.53–2.18, 2.02–1.50, 1.50–1.18.

2D ^{1}H-^{1}H NOESY NMR spectra

The as-prepared αCD-R_1-R_2 (2, 1, 1) hydrogels were swollen in water to eliminate excess KCl. The swollen hydrogels were cut into small pieces and dried with flowing air in a windy oven at 60 °C for 20 hours. The dried gels were immersed in D_2O in NMR tubes and analyzed by 2D ^{1}H-^{1}H NOESY NMR spectroscopy (600 MHz, 25 °C, mixing time = 500 ms) (**Figures S8–S13**).

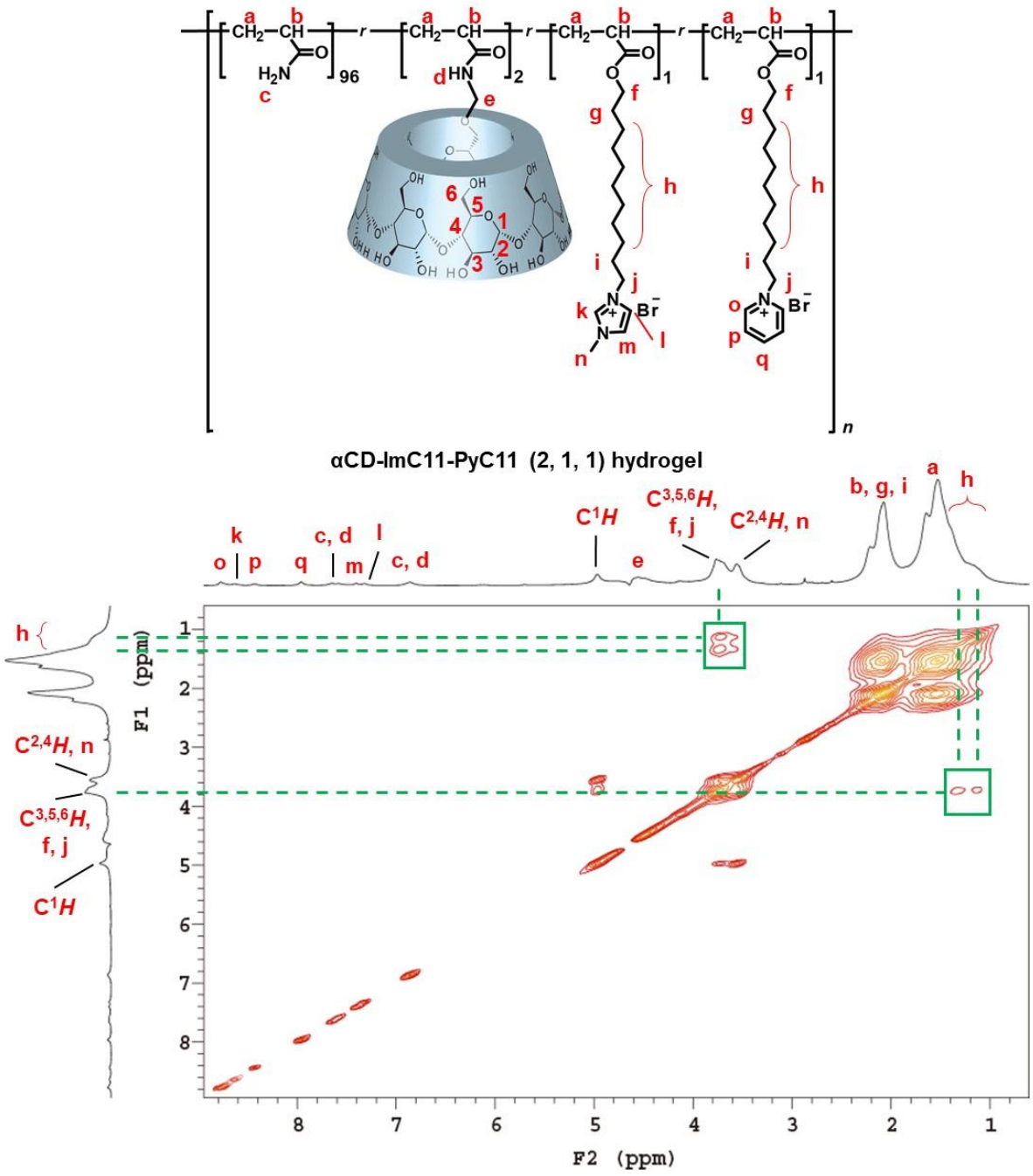

Figure S8. 600 MHz 2D ^{1}H-^{1}H NOESY NMR spectrum of the αCD-ImC11-PyC11 (2, 1, 1) hydrogel in D_2O at 25 °C. NOE correlation peaks between undecyl units and inner protons of αCDs are indicated with green boxes. To suppress the water peak, we performed presaturation and diffusion filter processes.

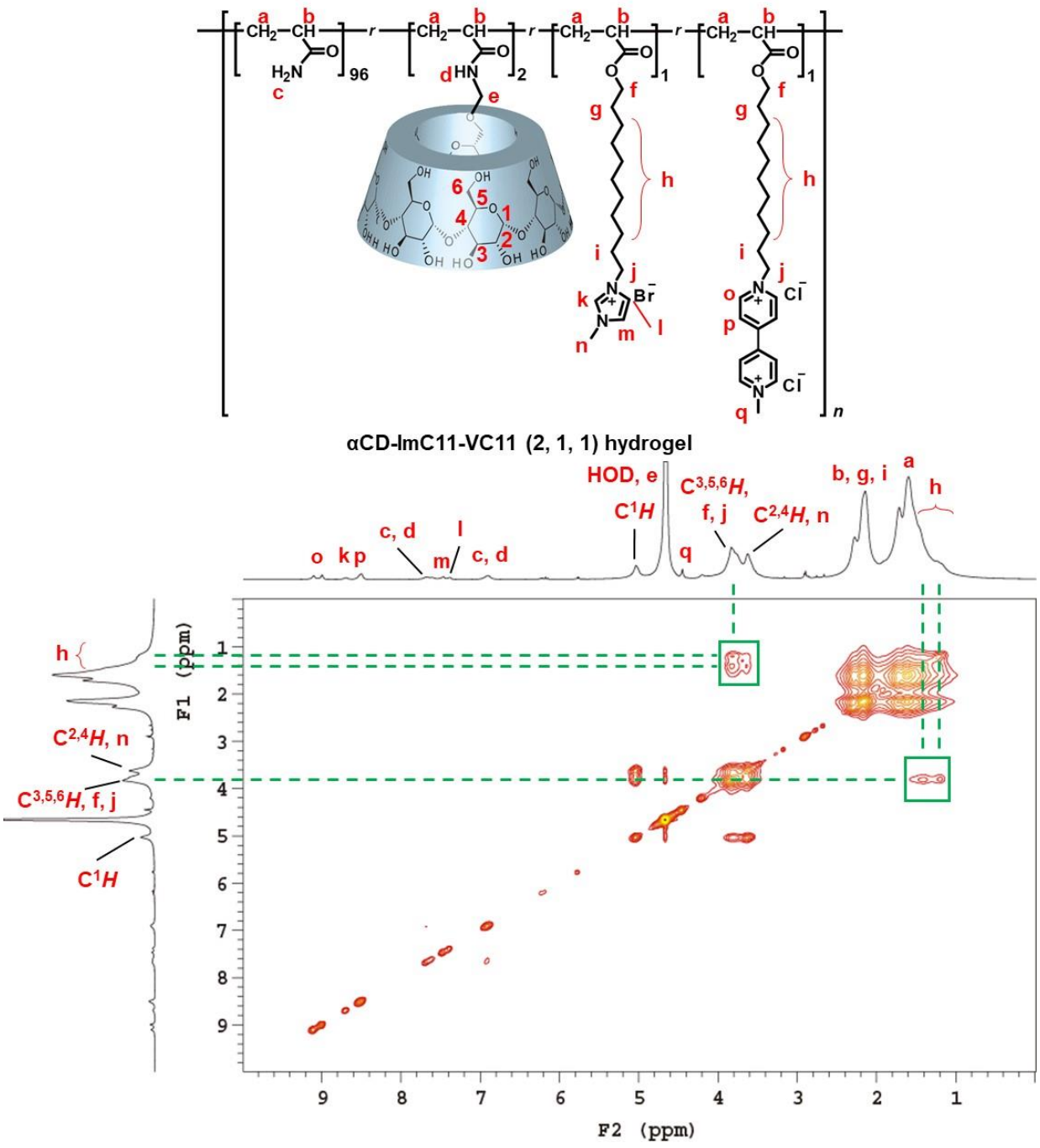

Figure S9. 600 MHz 2D ^{1}H-^{1}H NOESY NMR spectrum of the αCD-ImC11-VC11 (2, 1, 1) hydrogel in D_2O at 25 °C. NOE correlation peaks between undecyl units and inner protons of αCDs are indicated with green boxes.

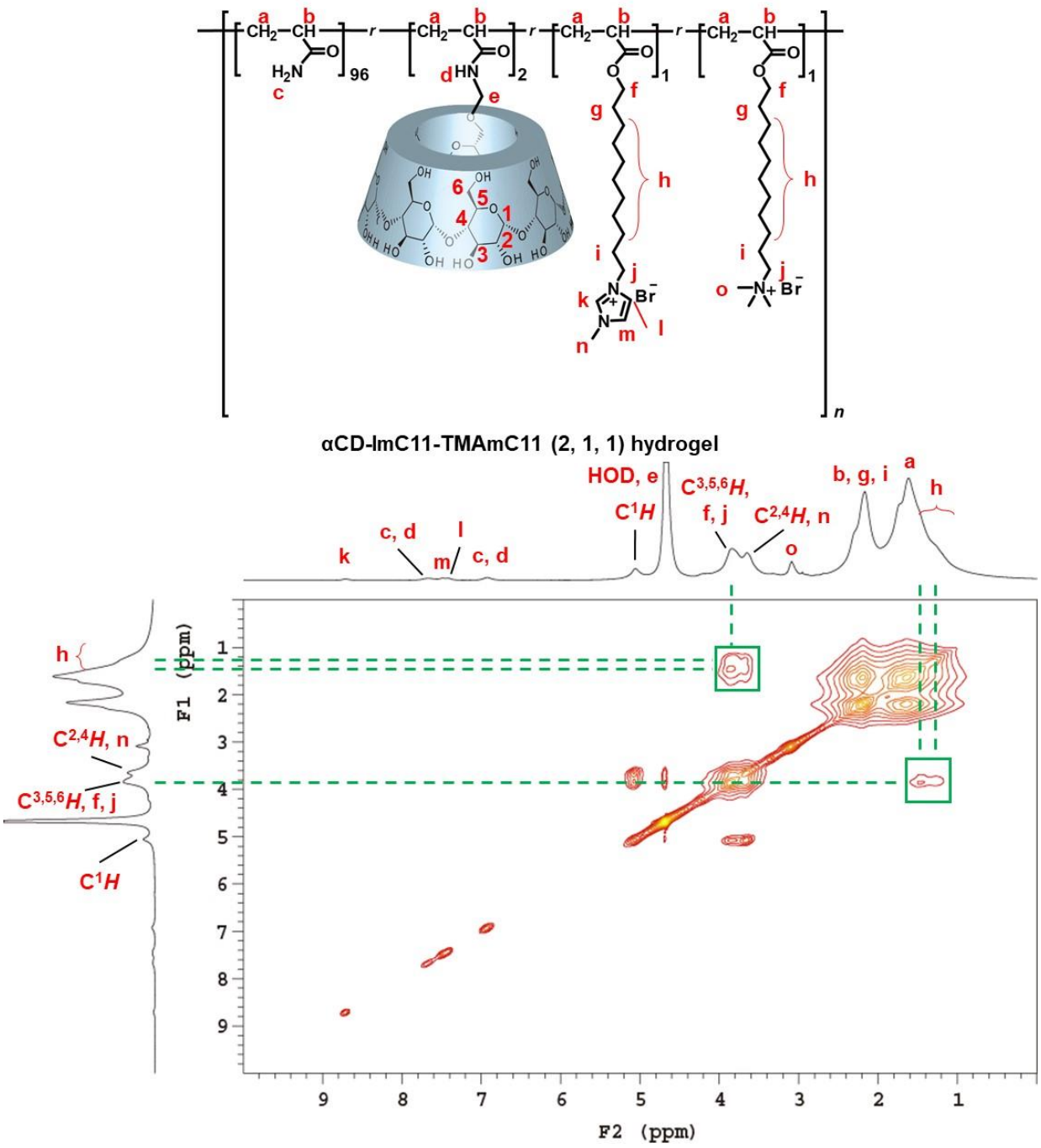

Figure S10. 600 MHz 2D ^{1}H-^{1}H NOESY NMR spectrum of the αCD-ImC11-TMAmC11 (2, 1, 1) hydrogel in D_2O at 25 °C. NOE correlation peaks between undecyl units and inner protons of αCDs are indicated with green boxes.

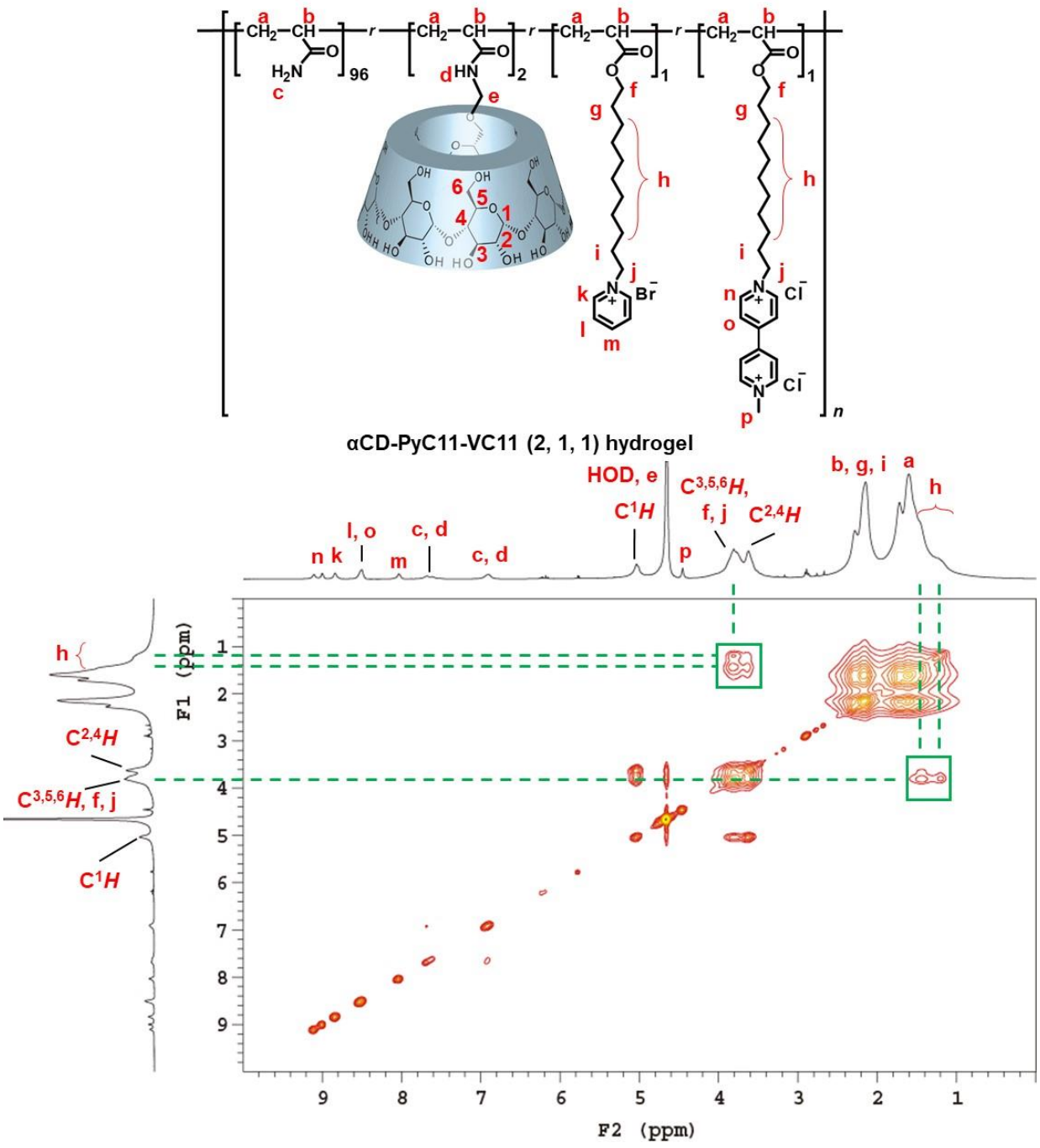

Figure S11. 600 MHz 2D ^{1}H-^{1}H NOESY NMR spectrum of the αCD-PyC11-VC11 (2, 1, 1) hydrogel in D_2O at 25 °C. NOE correlation peaks between undecyl units and inner protons of αCDs are indicated with green boxes.

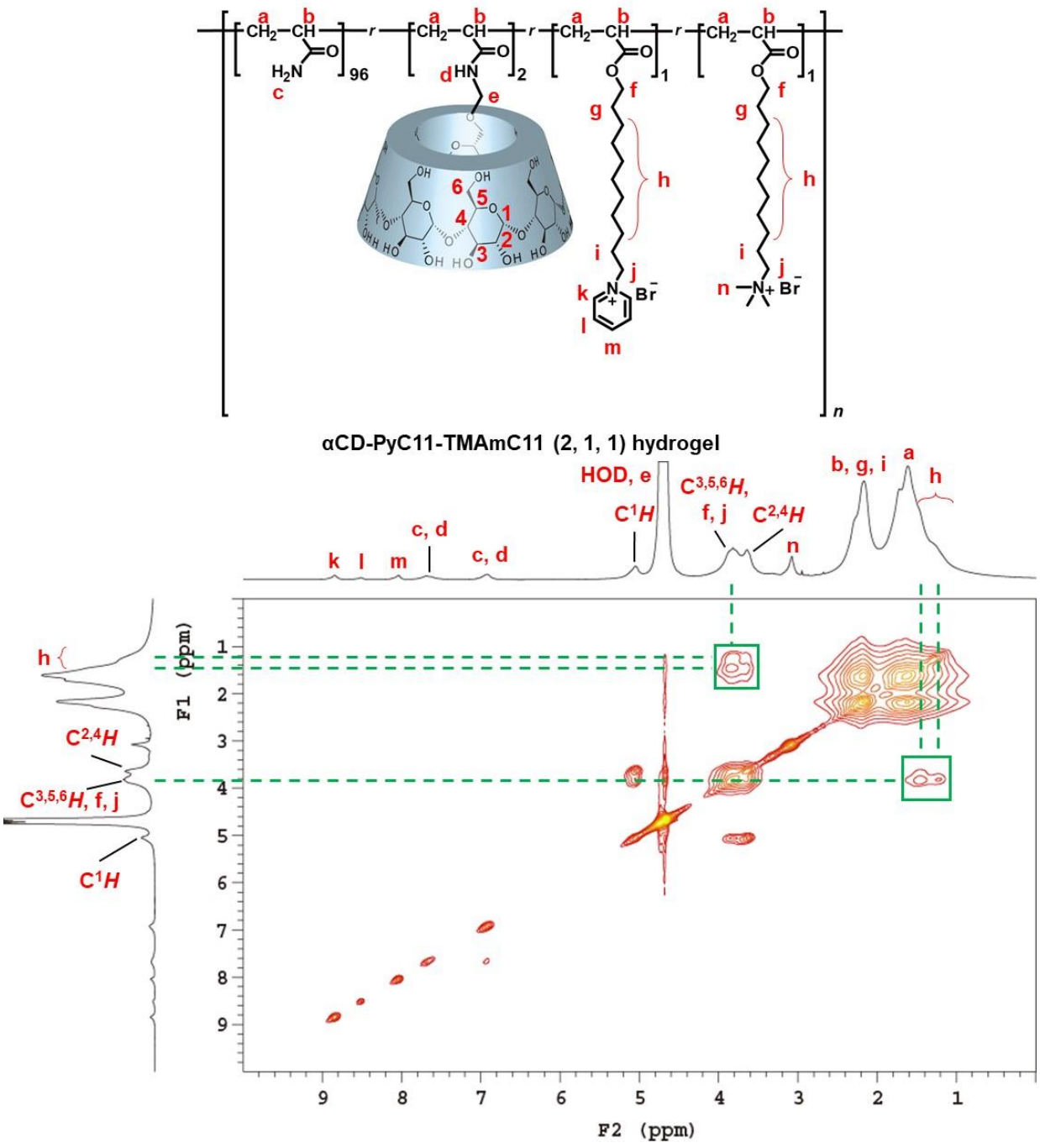

Figure S12. 600 MHz 2D ^{1}H-^{1}H NOESY NMR spectrum of the αCD-PyC11-TMAmC11 (2, 1, 1) hydrogel in D_2O at 25 °C. NOE correlation peaks between undecyl units and inner protons of αCDs are indicated with green boxes.

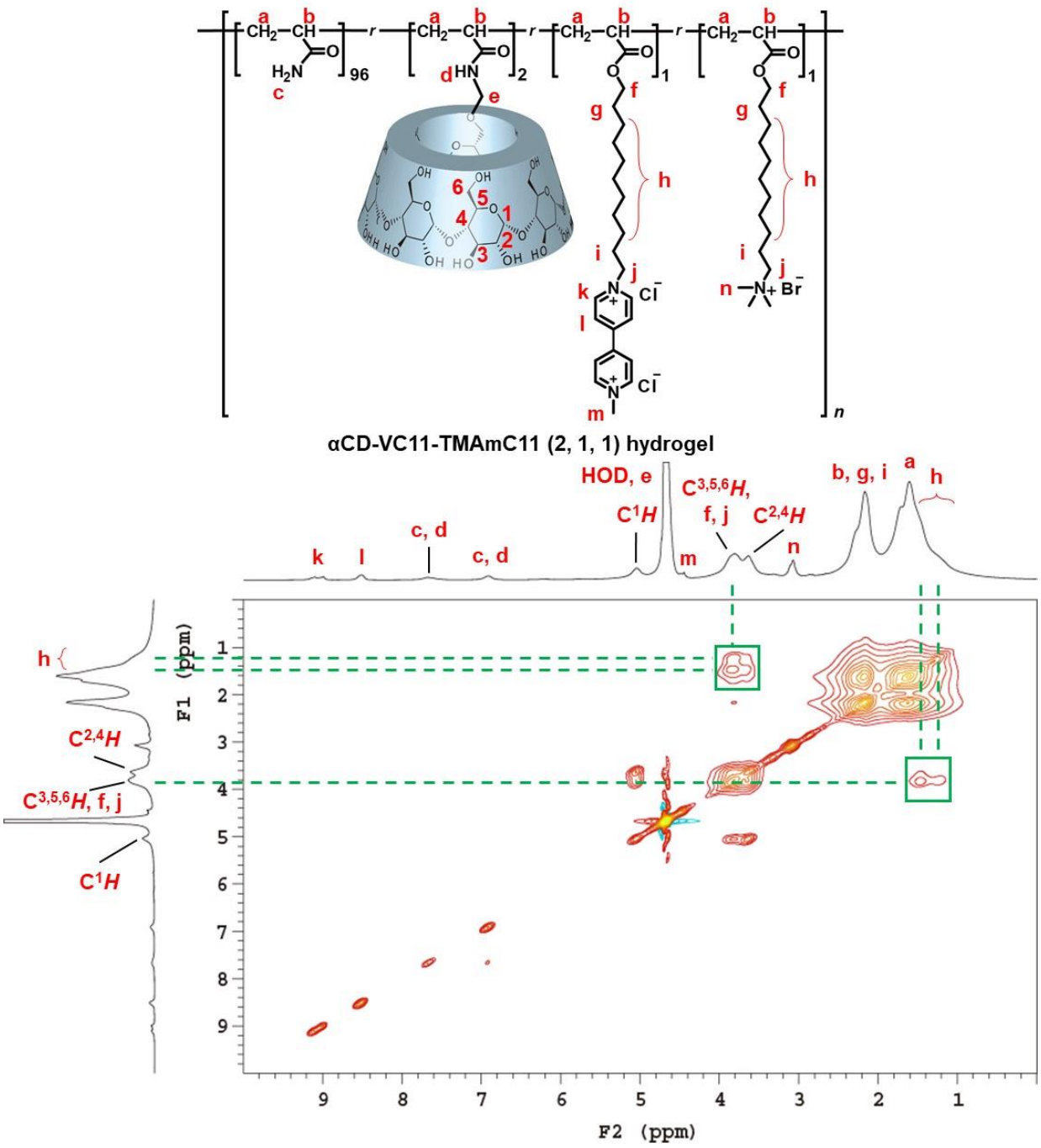

Figure S13. 600 MHz 2D ^{1}H-^{1}H NOESY NMR spectrum of the αCD-VC11-TMAmC11 (2, 1, 1) hydrogel in D_2O at 25 °C. NOE correlation peaks between undecyl units and inner protons of αCDs are indicated with green boxes.

4. Results of tensile tests on the αCD-R_1-R_2 hydrogels

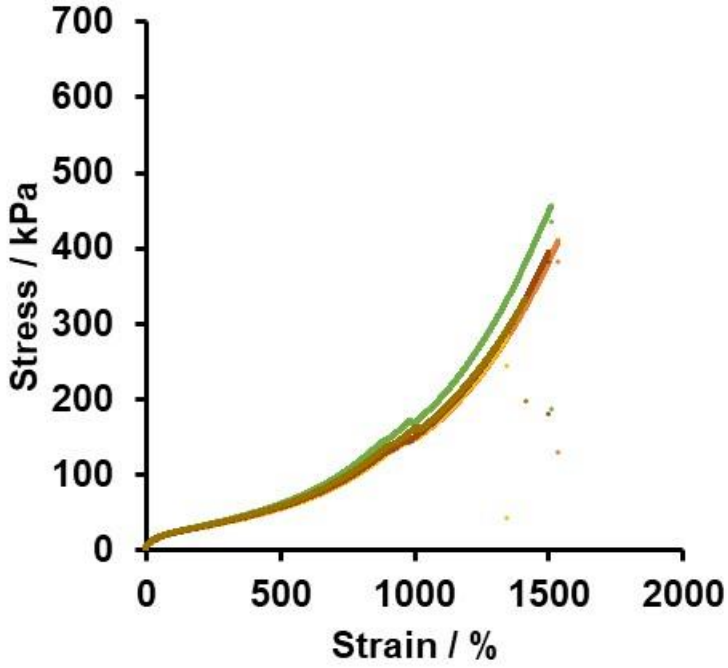

Figure S14. Stress–strain curves of the αCD-ImC11-PyC11 (2, 1, 1) hydrogel at 25 °C at a tensile rate of 1.0 mm/s (n = 5).

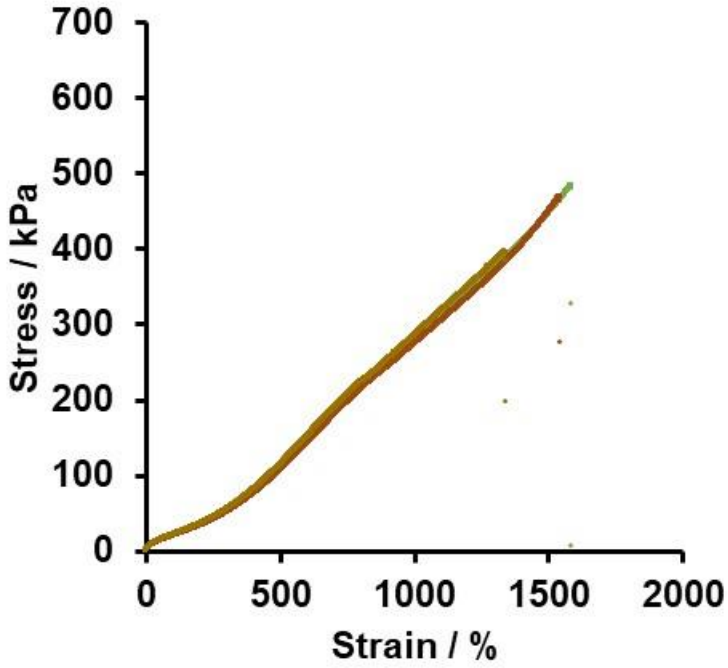

Figure S15. Stress–strain curves of the αCD-ImC11-VC11 (2, 1, 1) hydrogel at 25 °C at a tensile rate of 1.0 mm/s (n = 3).

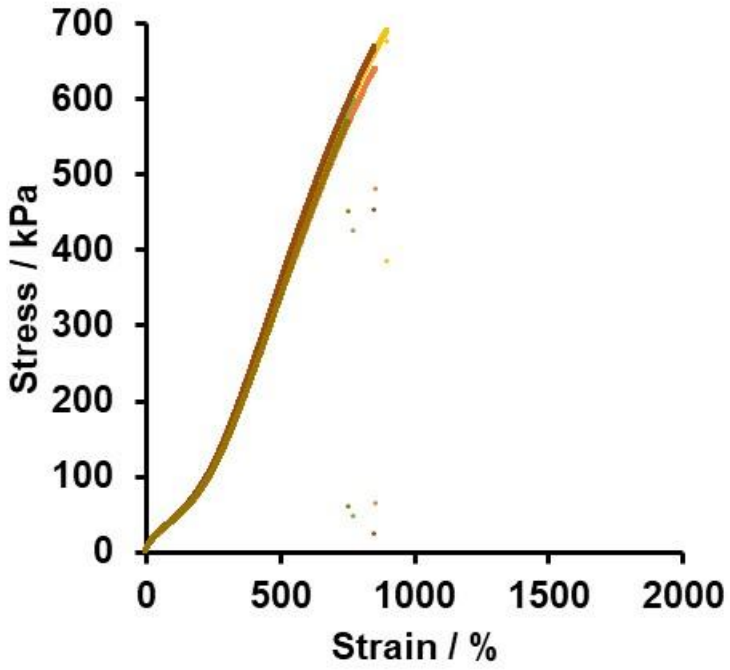

Figure S16. Stress–strain curves of the αCD-ImC11-TMAmC11 (2, 1, 1) hydrogel at 25 ºC at a tensile rate of 1.0 mm/s (n = 5).

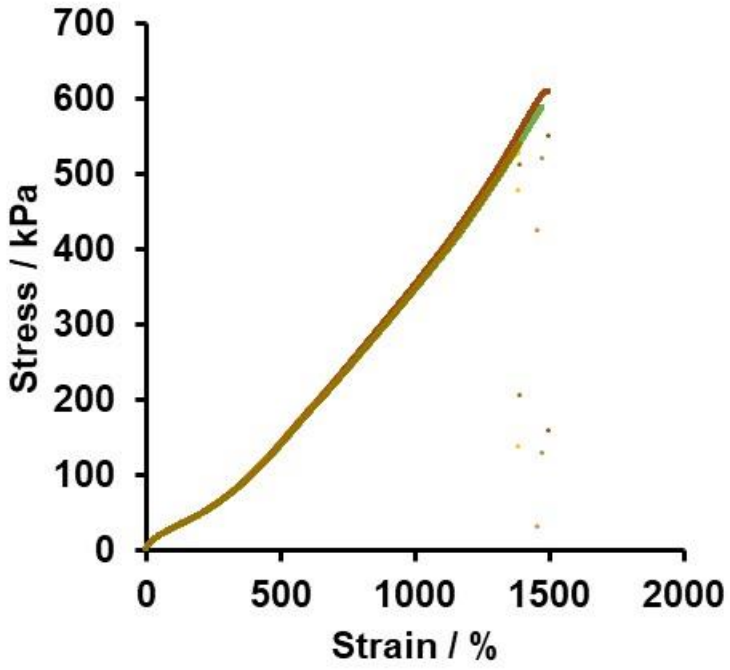

Figure S17. Stress–strain curves of the αCD-PyC11-VC11 (2, 1, 1) hydrogel at 25 ºC at a tensile rate of 1.0 mm/s (n = 5).

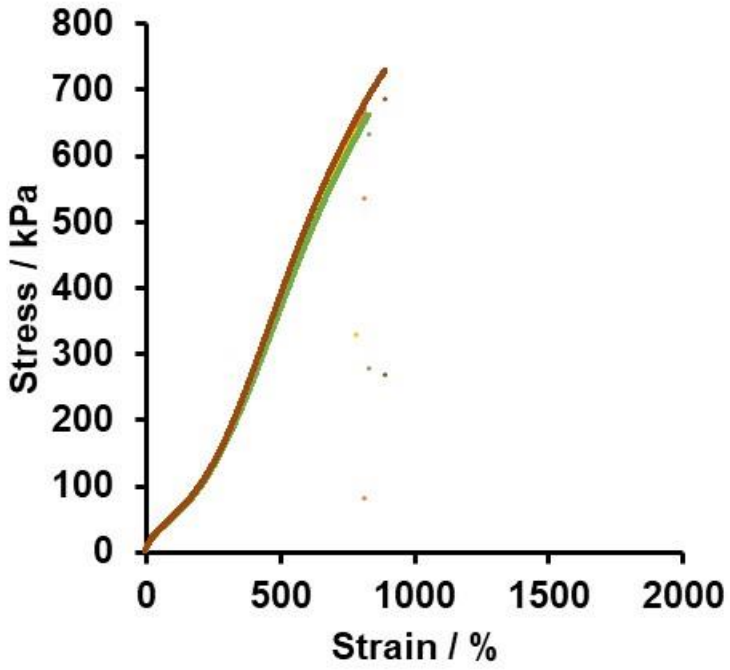

Figure S18. Stress–strain curves of the αCD-PyC11-TMAmC11 (2, 1, 1) hydrogel at 25 ºC at a tensile rate of 1.0 mm/s (n = 4).

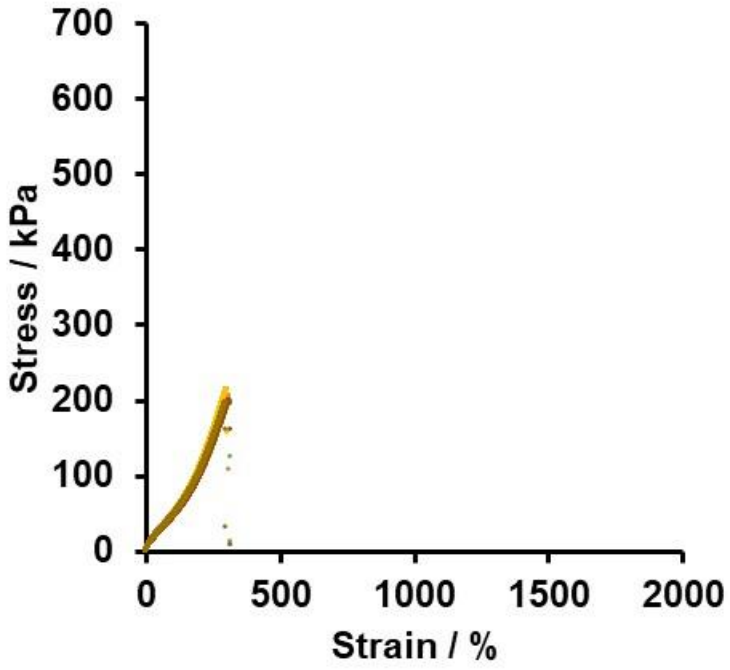

Figure S19. Stress–strain curves of the αCD-VC11-TMAmC11 (2, 1, 1) hydrogel at 25 ºC at a tensile rate of 1.0 mm/s (n = 5).

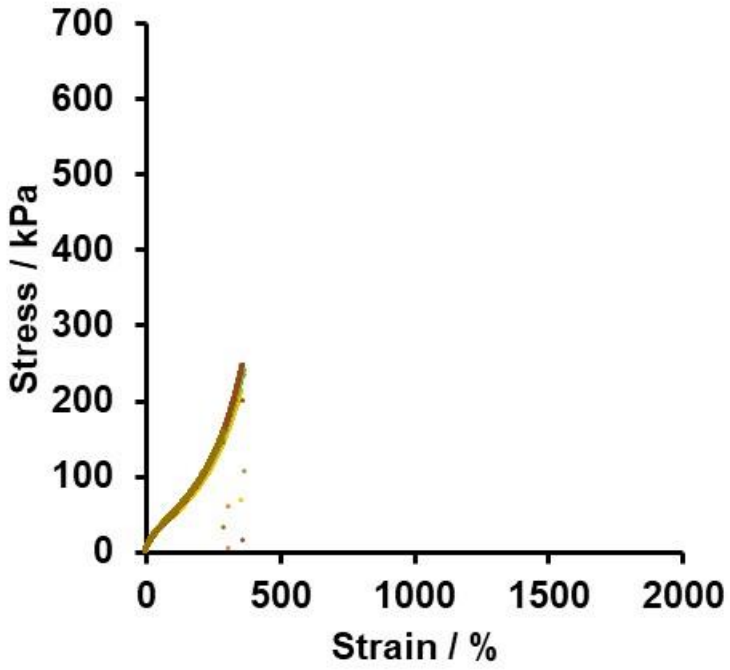

Figure S20. Stress–strain curves of the αCD-PyC11-MBAAm (1, 1, 0.5) hydrogel at 25 °C at a tensile rate of 1.0 mm/s (n = 5).

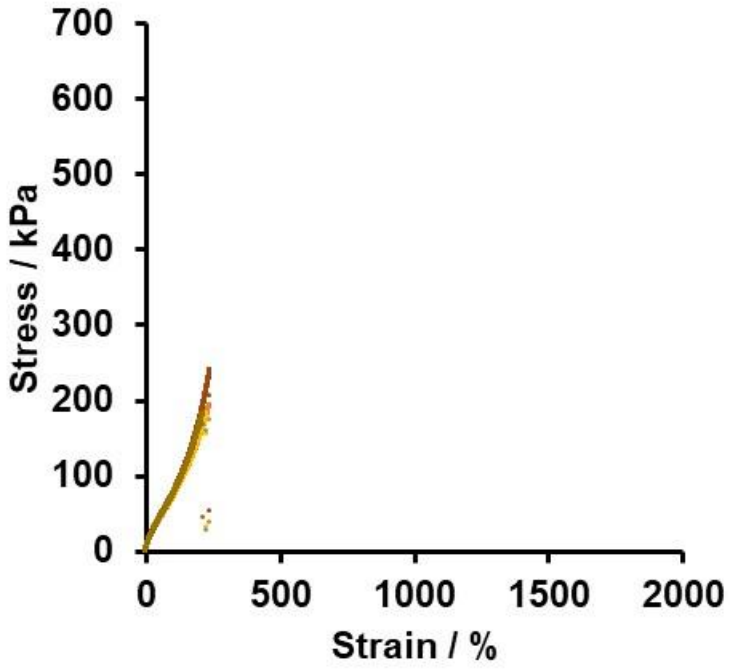

Figure S21. Stress–strain curves of the αCD-PyC11-MBAAm (1, 1, 1) hydrogel at 25 °C at a tensile rate of 1.0 mm/s (n = 5).

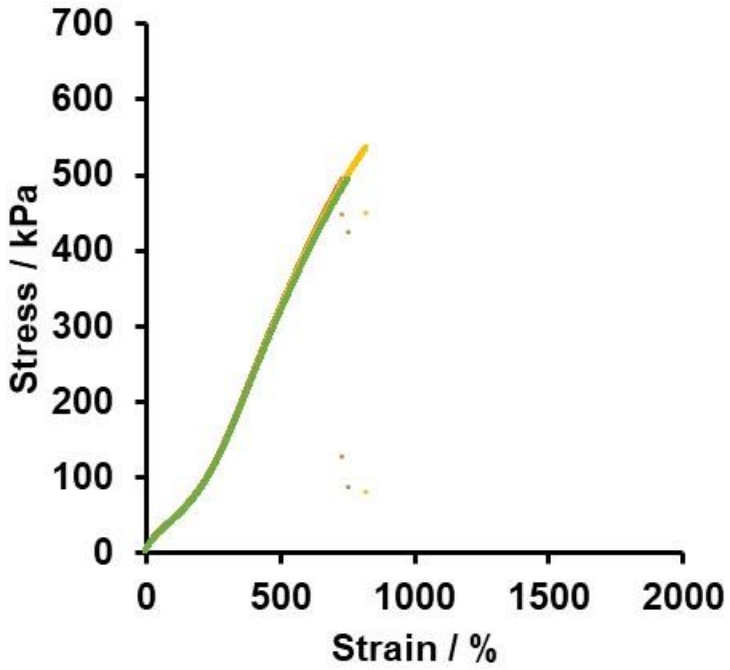

Figure S22. Stress–strain curves of the αCD-PyC11-VC11-TMAmC11 (2, 0.67, 0.67, 0.67) hydrogel at 25 °C at a tensile rate of 1.0 mm/s (n = 3).

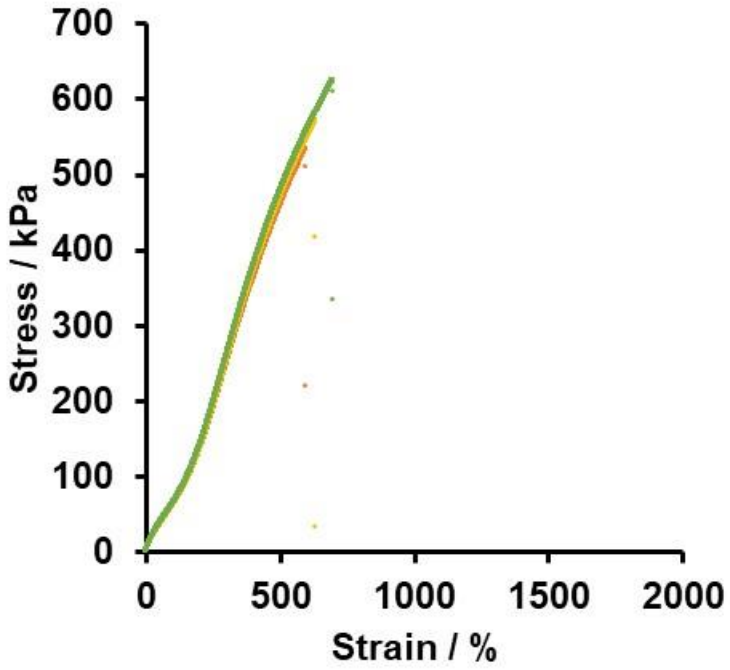

Figure S23. Stress–strain curves of the αCD-PyC11-VC11-TMAmC11 (3, 1, 1, 1) hydrogel at 25 °C at a tensile rate of 1.0 mm/s (n = 3).

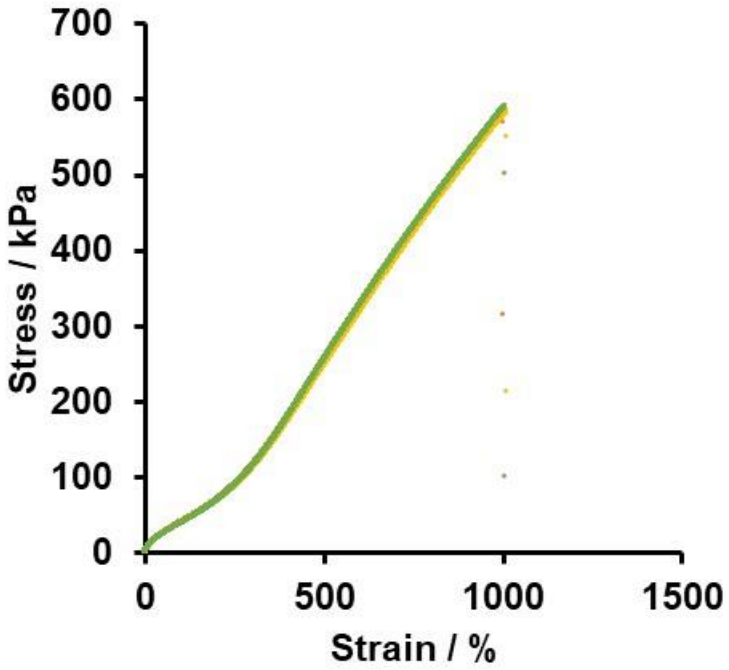

Figure S24. Stress–strain curves of the αCD-PyC11-VC11-TMAmC11 (2, 1, 0.5, 0.5) hydrogel at 25 °C at a tensile rate of 1.0 mm/s (n = 3).

5. Results of cyclic tensile tests on the αCD-R_1-R_2 and αCD-R hydrogels

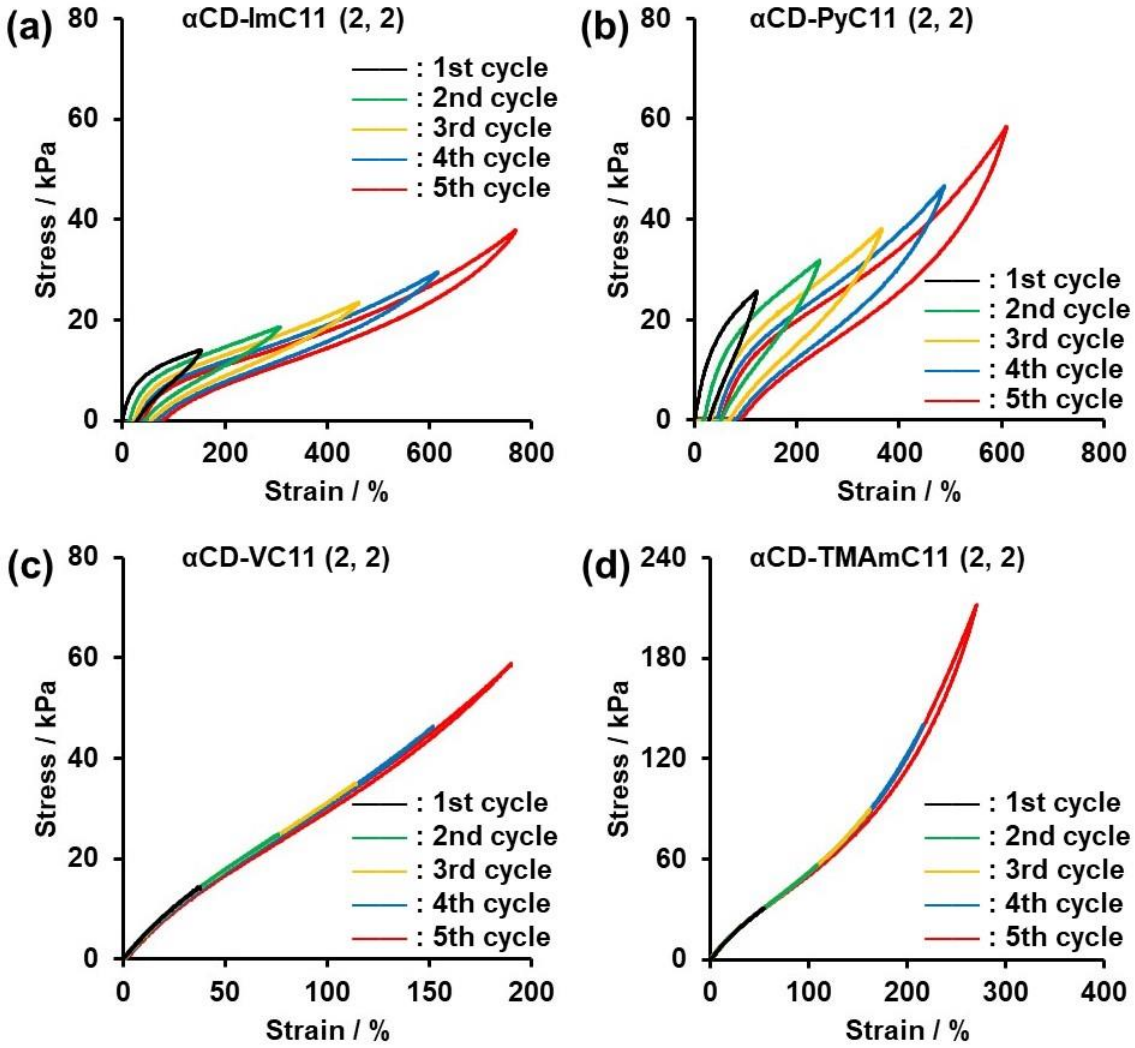

Figure S25. Cyclic stress–strain curves of **(a)** αCD-ImC11 (2, 2), **(b)** αCD-PyC11 (2, 2), **(c)** αCD-VC11 (2, 2), and **(d)** αCD-TMAmC11 (2, 2) hydrogels. Maximum strains were set to 16%, 32%, 48%, 64% and 80% of the fracture strain of each gel.

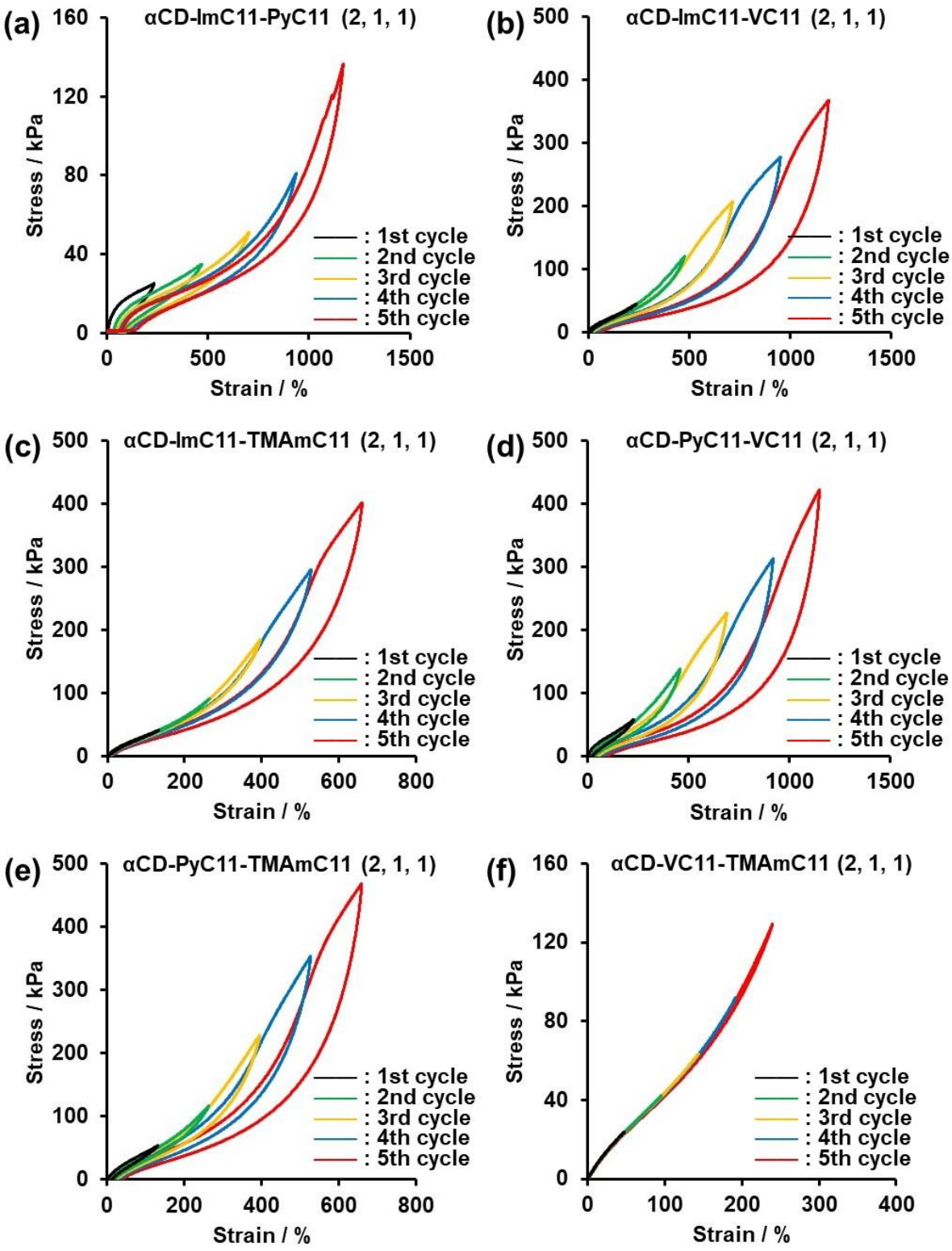

Figure S26. Cyclic stress–strain curves of **(a)** αCD-ImC11-PyC11 (2, 1, 1), **(b)** αCD-ImC11-VC11 (2, 1, 1), **(c)** αCD-ImC11-TMAmC11 (2, 1, 1), **(d)** αCD-PyC11-VC11 (2, 1, 1), **(e)** αCD-PyC11-TMAmC11 (2, 1, 1), and **(f)** αCD-VC11-TMAmC11 (2, 1, 1) hydrogels. Maximum strains were set to 16%, 32%, 48%, 64% and 80% of the fracture strain of each gel.

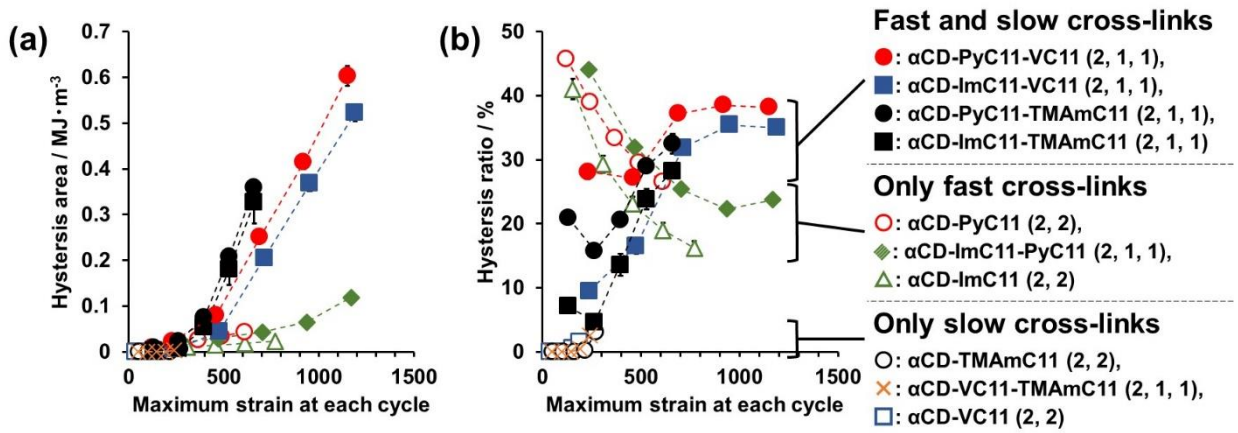

Figure S27. (a) Relation between hysteresis areas and maximum strains at each cycle for the αCD-R_1-R_2 (2, 1, 1) and αCD-R (2, 2) hydrogels. **(b)** Relation between hysteresis ratios and maximum strains at each cycle for the αCD-R_1-R_2 (2, 1, 1) and αCD-R (2, 2) hydrogels.

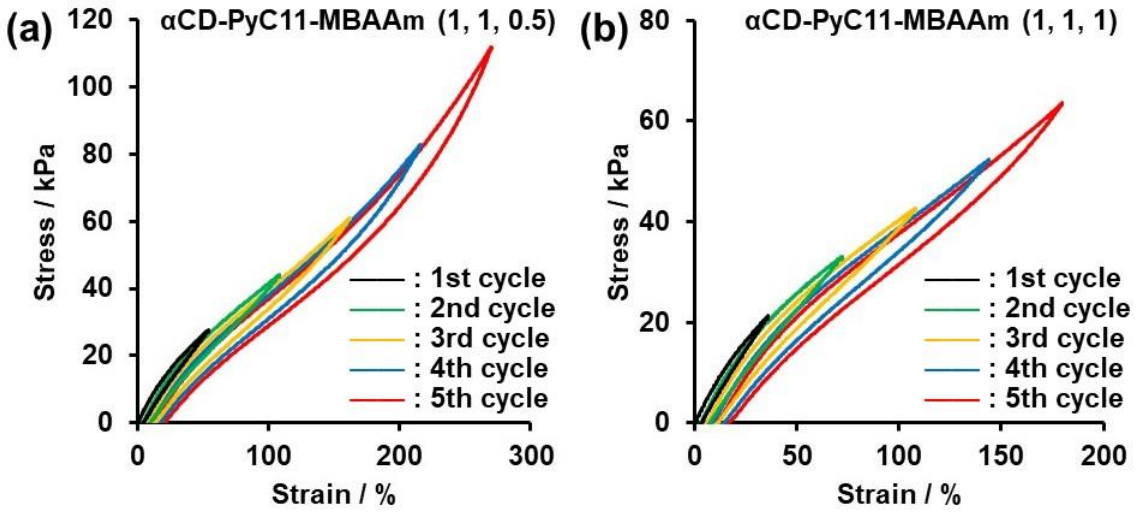

Figure S28. Cyclic stress–strain curves of **(a)** the αCD-PyC11-MBAAm (1, 1, 0.5) and **(b)** the αCD-PyC11-MBAAm (1, 1, 1) hydrogels. Maximum strains were set to 16%, 32%, 48%, 64% and 80% of the fracture strain of each gel.

6. Linear viscoelastic measurements of the αCD-R_1-R_2 hydrogels

Dynamic viscoelastic measurements of sheet-like samples with thicknesses of ~ 1 mm were performed with an Anton Paar MCR302 rheometer (**Figures S29–S34**). An angular frequency (ω) sweep was performed from 0.1 to 100 rad/s using a parallel-plate fixture 8 mm in diameter at a temperature range of 0–45 °C (**Figures S29c–S34c**). The oscillatory shear strain amplitudes (γ) for all tests were within the range of linear viscoelasticity. The results for the αCD-R_1-R_2 (2, 1, 1) hydrogels at different temperatures and frequencies followed the time-temperature superposition principle to give master curves. We suppose that temperature only changed the rate of relaxation while keeping the microstructure the mode of molecular motion that induced viscoelastic relaxation unchanged in the experimental window. Therefore, the time-temperature superposition was applicable.

Figures S29d–S34d show the master curves for the storage modulus (G'), loss modulus (G'') and loss factor (tan δ) referenced at 25 °C and the Arrhenius plot depicting the temperature dependence of the shift factors (a_T) for each sample. Relaxation modes (G_p and τ_p) were estimated by fitting master curves of G' and G'' with the generalized Maxwellian model (eqs. (4) and (5)), except for the plateau of the αCD-VC11-TMAmC11 (2, 1, 1) hydrogel. The results for the αCD-R (2, 2) hydrogels were reported in our previous work.[3] Second-order average relaxation times ($<\tau>_w$) of the αCD-R (2, 2) hydrogels corresponding to the lifetimes of the αCD-R cross-links were calculated by using eq. (6).

$$G' = \sum_{p\geq 1}^{N} G_p \frac{\omega^2 {\tau_p}^2}{1+\omega^2 {\tau_p}^2} + G_N \quad (4)$$

$$G'' = \sum_{p\geq 1}^{N} G_p \frac{\omega \tau_p}{1+\omega^2 {\tau_p}^2} \quad (5)$$

$$\langle \tau \rangle_{\mathrm{w}} = \frac{\sum_{p\geq 1}^{N} G_p {\tau_p}^2}{\sum_{p\geq 1}^{N} G_p \tau_p} \quad (6)$$

G_p: Relaxation strength in p^{th} relaxation mode.

τ_p: Relaxation time in p^{th} relaxation mode.

G_{N}: Terminal modulus.

The apparent activation energy ΔE_{a} was calculated from the Arrhenius equation (7), where a_{T} is the shift factor, R is the ideal gas constant, and A is a constant. Equation (7) was converted to equation (8). **Figures S29e-S34e** show Arrhenius plots of the logarithm of a_{T} and the inverse of T using eq. (8).

$$a_{\mathrm{T}} = A e^{\frac{\Delta E_{\mathrm{a}}}{RT}} \quad (7)$$

$$\ln a_{\mathrm{T}} = \frac{\Delta E_{\mathrm{a}}}{R}\left(\frac{1}{T} - \frac{1}{T_0}\right) \quad (8)$$

To detect long relaxation times of the αCD-R_1-R_2 (2, 1, 1) hydrogels, stress-relaxation tests were also performed with an MCR302 rheometer at 25 °C (**Figure S29f–S34f**). The relaxation modulus ($G(t)$) was fitted with the following equation (11):

$$G(t) = \sum_{p\geq 1}^{N} G_p e^{-\frac{t}{\tau_p}} + G_{\mathrm{N}} \quad (11)$$

Parameters G_{p}, τ_{p}, and G_{N} obtained from the master curves and stress-relaxation curves are summarized in **Tables S16–S26**.

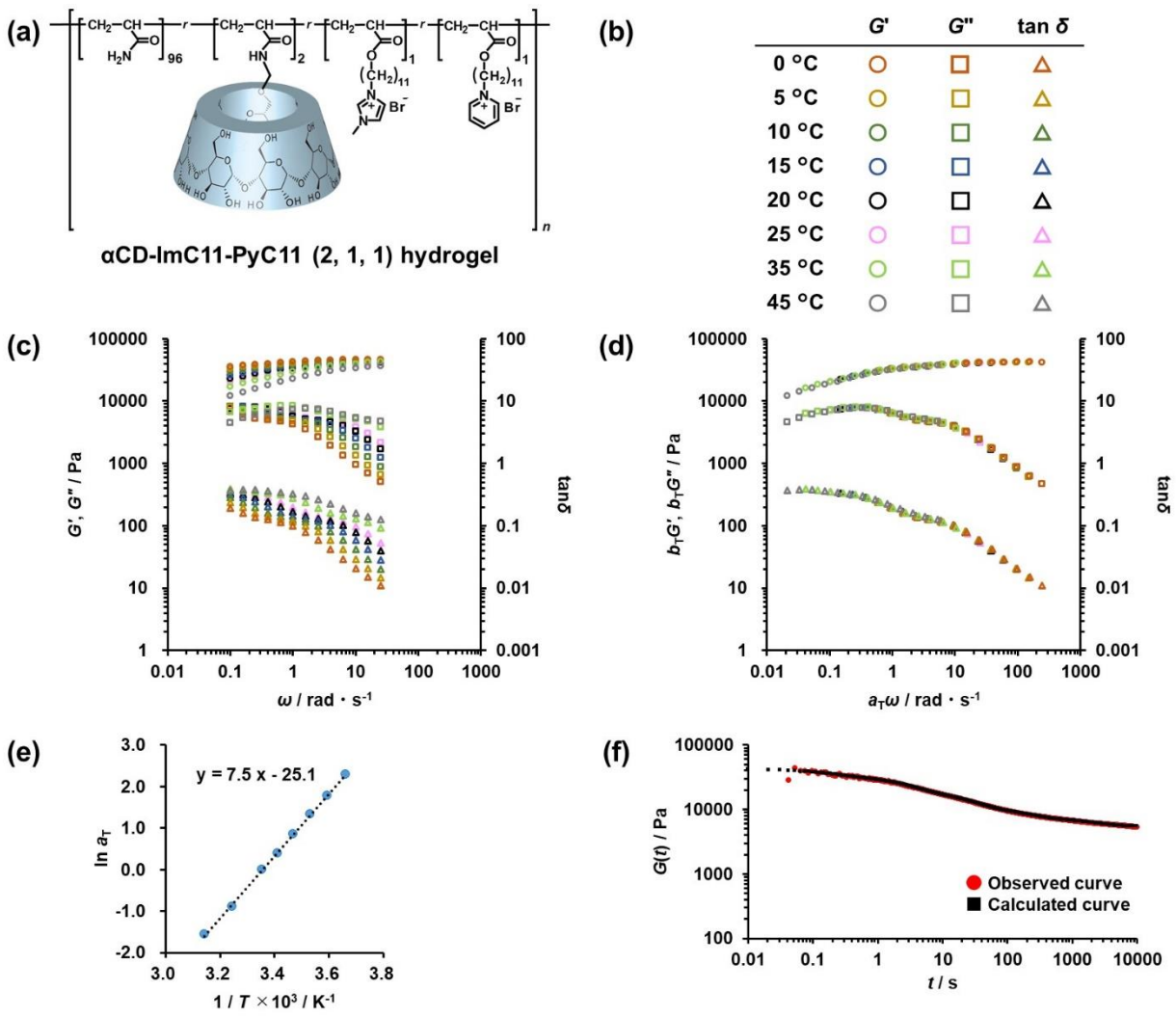

Figure S29. (a) Chemical structure of the αCD-ImC11-PyC11 (2, 1, 1) hydrogel. **(b)** Symbols for G', G'', and tanδ defined at each temperature. **(c)** Angular frequency dependence of G', G'', and tanδ (amplitude strain (γ) = 1%). **(d)** Master curves of G', G'', and tanδ for the αCD-ImC11-PyC11 (2, 1, 1) hydrogel referenced to 25 °C. **(e)** The Arrhenius plot of a_T used for superposition. **(f)** The stress-relaxation curve of the αCD-ImC11-PyC11 (2, 1, 1) hydrogel (γ = 3%, T = 25 °C) and curve fitting.

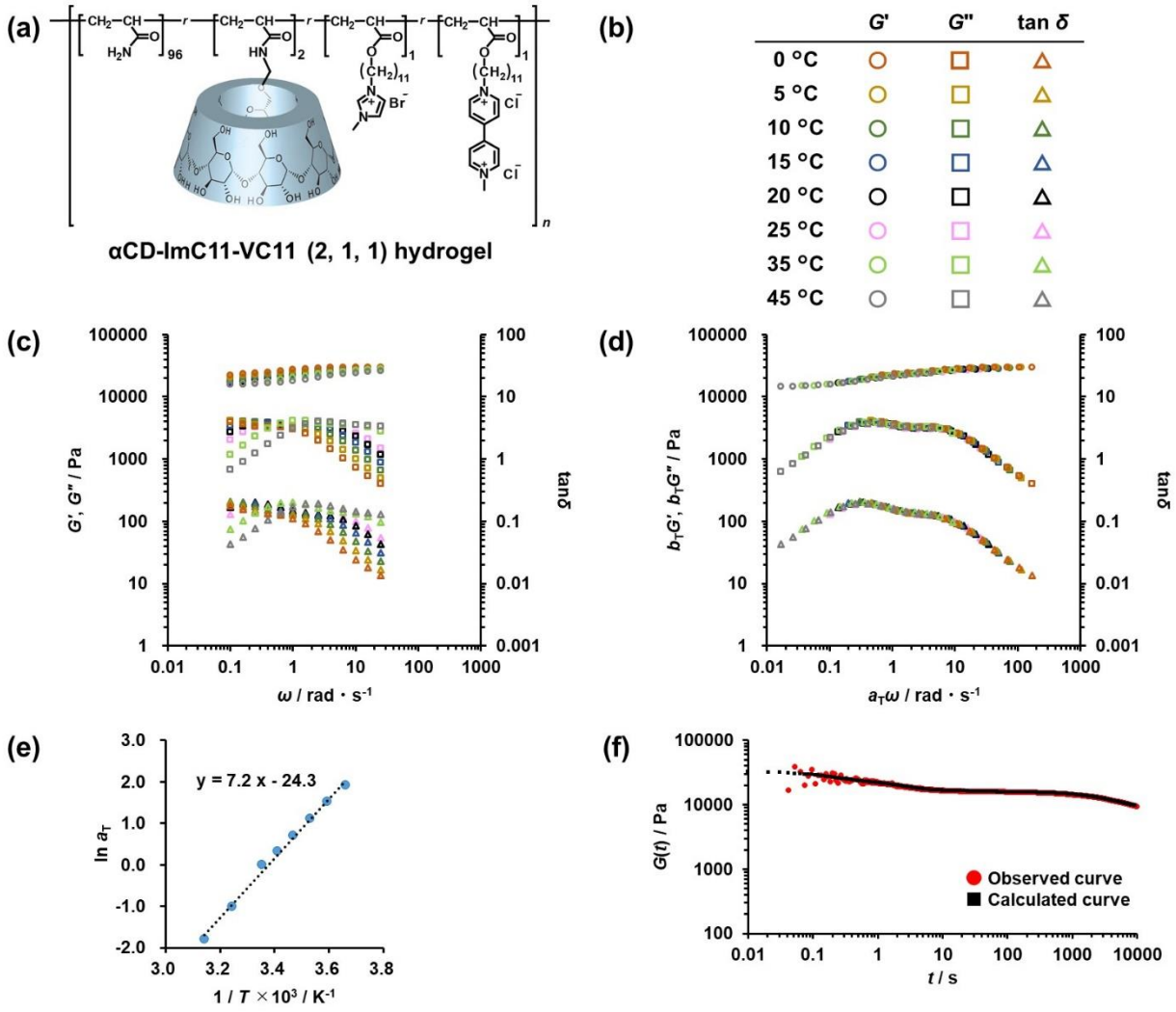

Figure S30. (a) Chemical structure of the αCD-ImC11-VC11 (2, 1, 1) hydrogel. **(b)** Symbols for G', G'', and tanδ defined at each temperature. **(c)** Angular frequency dependence of G', G'', and tanδ (γ = 1%). **(d)** Master curves of G', G'', and tanδ for the αCD-ImC11-VC11 (2, 1, 1) hydrogel referenced to 25 °C. **(e)** Arrhenius plot of a_T used for superposition. **(f)** Stress-relaxation curve of the αCD-ImC11-VC11 (2, 1, 1) hydrogel (γ = 3%, T = 25 °C) and curve fitting.

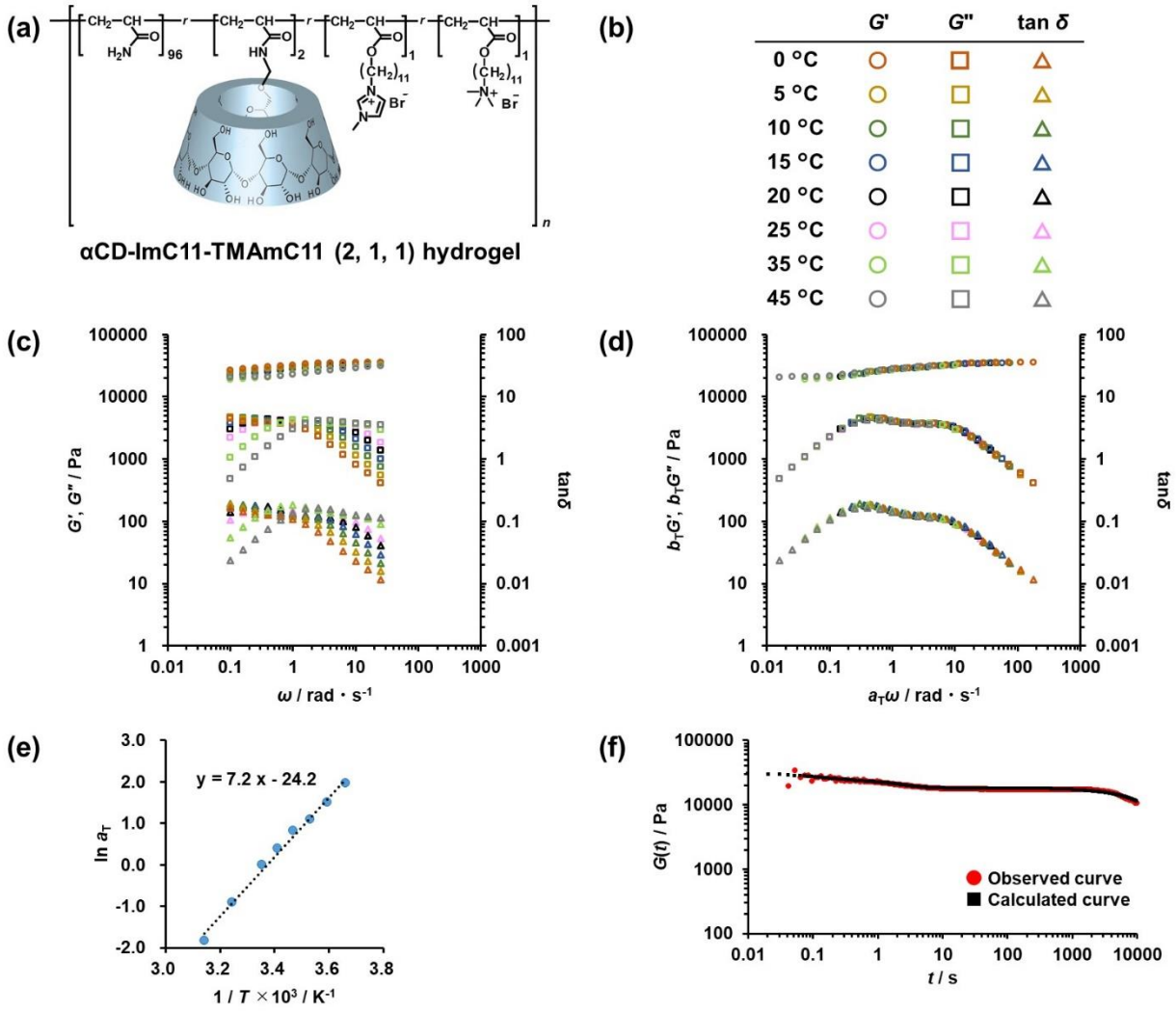

Figure S31. (a) Chemical structure of the αCD-ImC11-TMAmC11 (2, 1, 1) hydrogel. **(b)** Symbols for G', G'', and tanδ defined at each temperature. **(c)** Angular frequency dependence of G', G'', and tanδ (γ = 1%). **(d)** Master curves of G', G'', and tanδ for the αCD-ImC11-TMAmC11 (2, 1, 1) hydrogel referenced to 25 °C. **(e)** Arrhenius plot of a_T used for superposition. **(f)** Stress-relaxation curve of the αCD-ImC11-TMAmC11 (2, 1, 1) hydrogel (γ = 3%, T = 25 °C) and curve fitting.

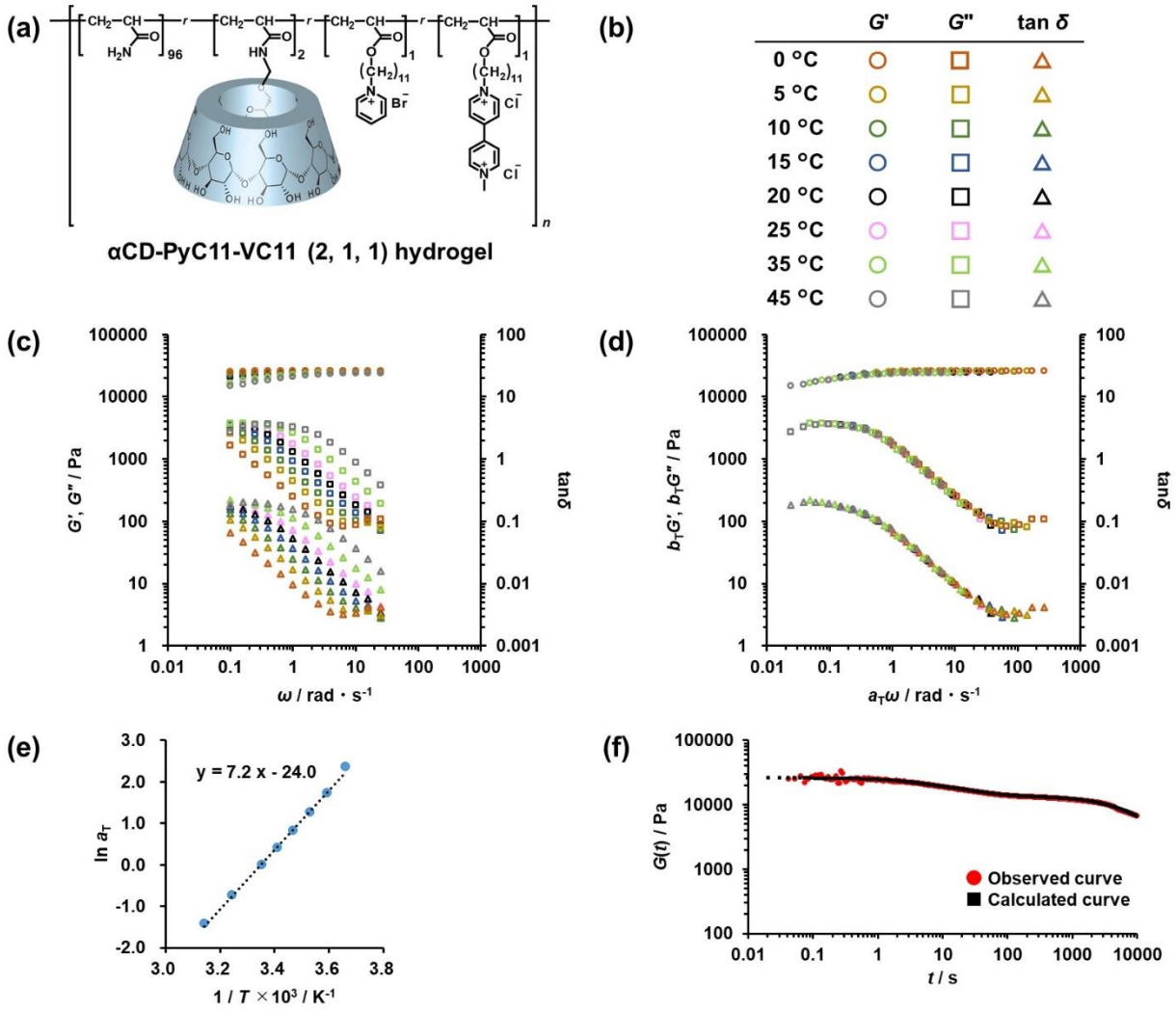

Figure S32. (a) Chemical structure of the αCD-PyC11-VC11 (2, 1, 1) hydrogel. **(b)** Symbols for G', G'', and tanδ defined at each temperature. **(c)** Angular frequency dependence of G', G'', and tanδ (γ = 1%). **(d)** Master curves of G', G'', and tanδ for the αCD-PyC11-VC11 (2, 1, 1) hydrogel referenced to 25 °C. **(e)** Arrhenius plot of a_T used for superposition. **(f)** Stress-relaxation curve of the αCD-PyC11-VC11 (2, 1, 1) hydrogel (γ = 3%, T = 25 °C) and curve fitting.

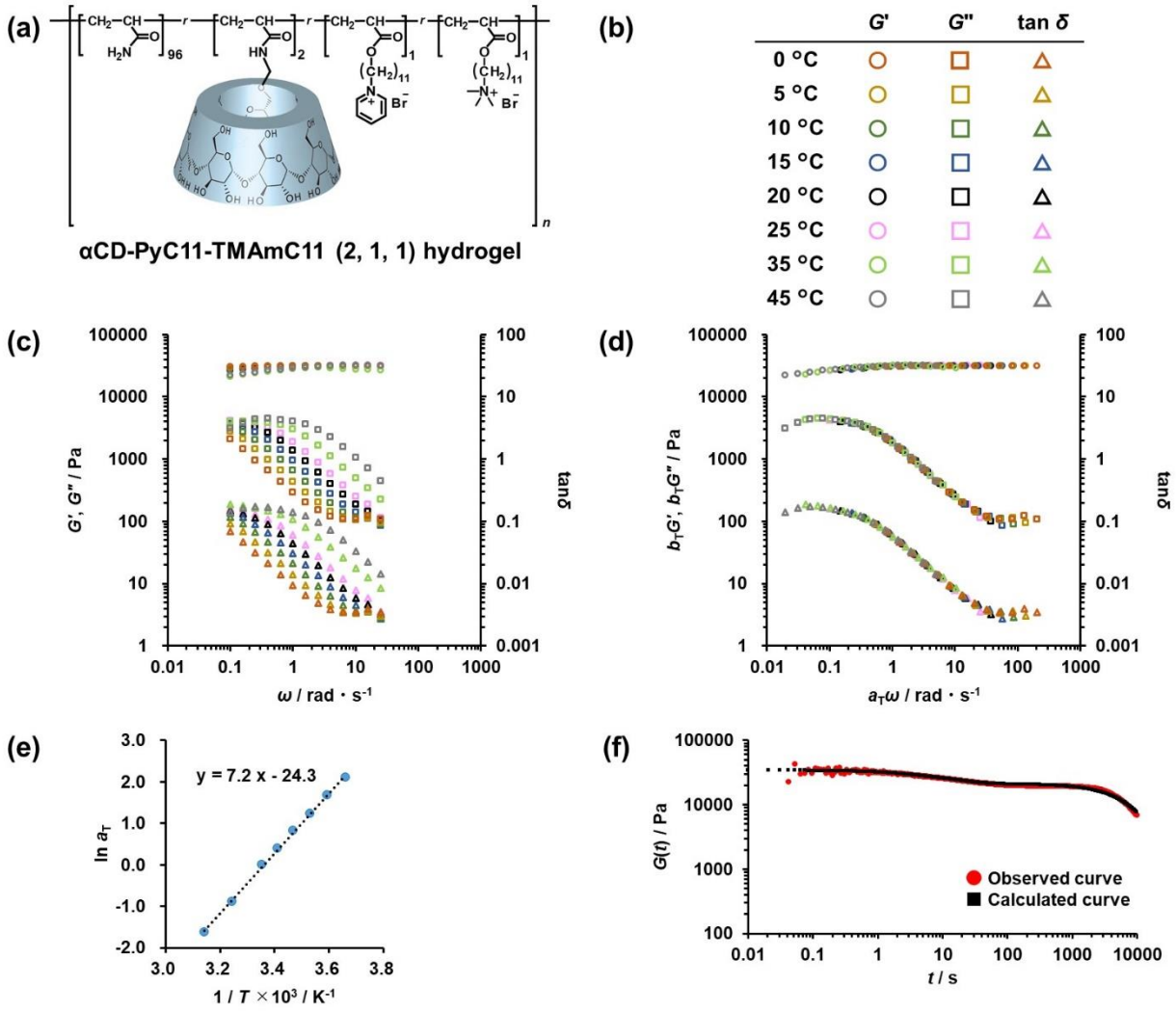

Figure S33. (a) Chemical structure of the αCD-PyC11-TMAmC11 (2, 1, 1) hydrogel. **(b)** Symbols for G', G'', and tanδ defined at each temperature. **(c)** Angular frequency dependence of G', G'', and tanδ (γ = 1%). **(d)** Master curves of G', G'', and tanδ for the αCD-PyC11-TMAmC11 (2, 1, 1) hydrogel referenced to 25 °C. **(e)** Arrhenius plot of a_T used for superposition. **(f)** Stress-relaxation curve of the αCD-PyC11-TMAmC11 (2, 1, 1) hydrogel (γ = 2%, T = 25 °C) and curve fitting.

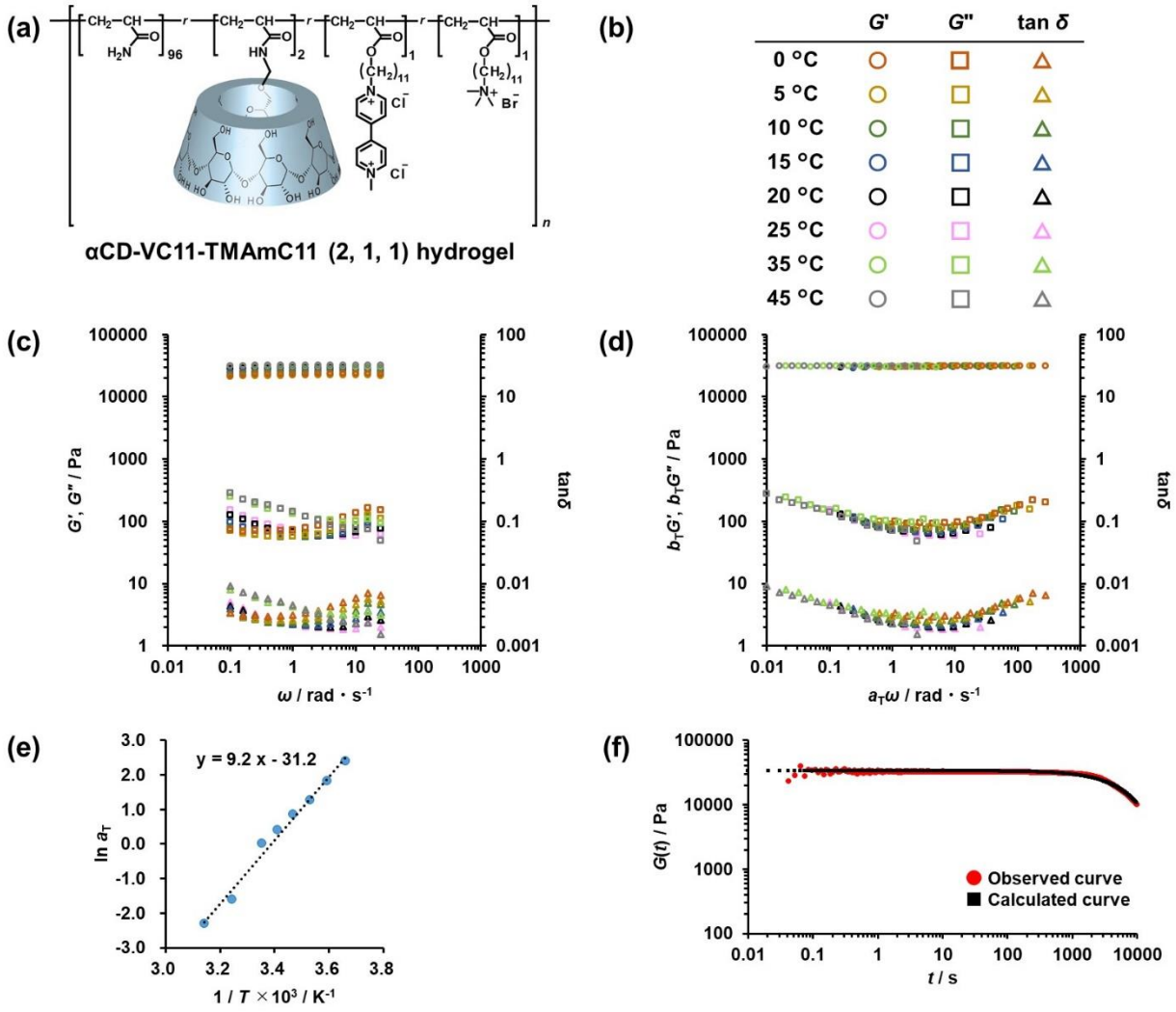

Figure S34. (a) Chemical structure of the αCD-VC11-TMAmC11 (2, 1, 1) hydrogel. **(b)** Symbols for G', G'', and tanδ defined at each temperature. **(c)** Angular frequency dependence of G', G'', and tanδ (γ = 0.8%). **(d)** Master curves of G', G'', and tanδ of the αCD-VC11-TMAmC11 (2, 1, 1) hydrogel referenced to 25 °C. **(e)** Arrhenius plot of a_T used for superposition. **(f)** Stress-relaxation curve of the αCD-VC11-TMAmC11 (2, 1, 1) hydrogel (γ = 2%, T = 25 °C) and curve fitting.

Table S16. Parameters G_p and τ_p used for fitting of the master curves of G' and G'' of the αCD-ImC11-PyC11 (2, 1, 1) hydrogel.

mode	1	2	3	4	5	6	7	G_N
G_p / Pa	7727	13037	10989	-	-	-	-	10492
τ_p / s	0.156	2.388	21.31	-	-	-	-	-

Table S17. Parameters G_p and τ_p used for fitting of the $G(t)$ of the αCD-ImC11-PyC11 (2, 1, 1) hydrogel.

mode	1	2	3	4	5	6	7	G_N
G_p / Pa	8863	13259	8734	3463	1937	-	-	5367
τ_p / s	0.200	2.843	25.45	189.2	2420	-	-	-

Table S18. Parameters G_p and τ_p used for fitting of the master curves of G' and G'' of the αCD-ImC11-VC11 (2, 1, 1) hydrogel.

mode	1	2	3	4	5	6	7	G_N
G_p / Pa	6025	7890	-	-	-	-	-	15008
τ_p / s	0.163	2.860	-	-	-	-	-	-

Table S19. Parameters G_p and τ_p used for fitting of $G(t)$ of the αCD-ImC11-VC11 (2, 1, 1) hydrogel.

mode	1	2	3	4	5	6	7	G_N
G_p / Pa	8000	7778	1019	7002	-	-	-	8660
τ_p / s	0.180	2.195	26.71	4650	-	-	-	-

Table S20. Parameters G_p and τ_p used for fitting of the master curves of G' and G'' of the αCD-ImC11-TMAmC11 (2, 1, 1) hydrogel.

mode	1	2	3	4	5	6	7	G_N
G_p / Pa	6270	8253	-	-	-	-	-	20455
τ_p / s	0.156	2.368	-	-	-	-	-	-

Table S21. Parameters G_p and τ_p used for fitting of $G(t)$ of the αCD-ImC11-TMAmC11 (2, 1, 1) hydrogel.

mode	1	2	3	4	5	6	7	G_N
G_p / Pa	5460	6885	17696	-	-	-	-	0
τ_p / s	0.127	2.214	21668	-	-	-	-	-

Table S22. Parameters G_p and τ_p used for fitting of the master curves of G' and G'' of the αCD-PyC11-VC11 (2, 1, 1) hydrogel.

mode	1	2	3	4	5	6	7	G_N
G_p / Pa	4467	6639	-	-	-	-	-	14146
τ_p / s	2.436	15.81	-	-	-	-	-	-

Table S23. Parameters G_p and τ_p used for fitting of $G(t)$ of the αCD-PyC11-VC11 (2, 1, 1) hydrogel.

mode	1	2	3	4	5	6	7	G_N
G_p / Pa	5161	5686	1410	8749	-	-	-	4463
τ_p / s	4.074	26.09	115.4	7014	-	-	-	-

Table S24. Parameters G_p and τ_p used for fitting of the master curves of G' and G'' of the αCD-PyC11-TMAmC11 (2, 1, 1) hydrogel.

mode	1	2	3	4	5	6	7	G_N
G_p / Pa	4800	7617	-	-	-	-	-	20000
τ_p / s	2.897	20.53	-	-	-	-	-	-

Table S25. Parameters G_p and τ_p used for fitting of $G(t)$ of the αCD-PyC11-TMAmC11 (2, 1, 1) hydrogel.

mode	1	2	3	4	5	6	7	G_N
G_p / Pa	4448	8392	20818	-	-	-	-	0
τ_p / s	2.409	17.12	9821	-	-	-	-	-

Table S26. Parameters G_p and τ_p used for fitting of $G(t)$ of the αCD-VC11-TMAmC11 (2, 1, 1) hydrogel.

mode	1	2	3	4	5	6	7	G_N
G_p / Pa	8801	2411	-	-	-	-	-	0
τ_p / s	7094	9403	-	-	-	-	-	-

The calculated ΔE_a values are summarized in **Table S27**. ΔE_a was almost the same for the αCD-R_1-R_2 (2, 1, 1) hydrogels. ΔE_a is one of the measures for the temperature dependence of relaxation, which is not the lifetime of the sticker. The αCD-R_1-R_2 (2, 1, 1) hydrogels showed similar values of ΔE_a, whereas their relaxation times were different. This result suggests that the lifetimes of the stickers are determined by the electrostatic instability of cation units, resulting in a direct effect on the viscoelastic relaxation time. Note that ΔE_a of the αCD-VC11-TMAmC11 (2, 1, 1) hydrogel was slightly higher than the others, which may be attributed to the elastic network cross-linked by the αCD-VC11 and αCD-TMAmC11 cross-links.

Table S27. Results for ΔE_a of the αCD-R_1-R_2 (2, 1, 1) hydrogels.

Sample	ΔE_a / kJ/mol
αCD-ImC11-PyC11 (2, 1, 1)	59.6
αCD-ImC11-VC11 (2, 1, 1)	59.7
αCD-ImC11-TMAmC11 (2, 1, 1)	59.6
αCD-PyC11-VC11 (2, 1, 1)	59.6
αCD-PyC11-TMAmC11 (2, 1, 1)	60.1
αCD-VC11-TMAmC11 (2, 1, 1)	76.4

7. Small angle X-ray scattering measurements of the αCD-R_1-R_2 and αCD-R hydrogels.

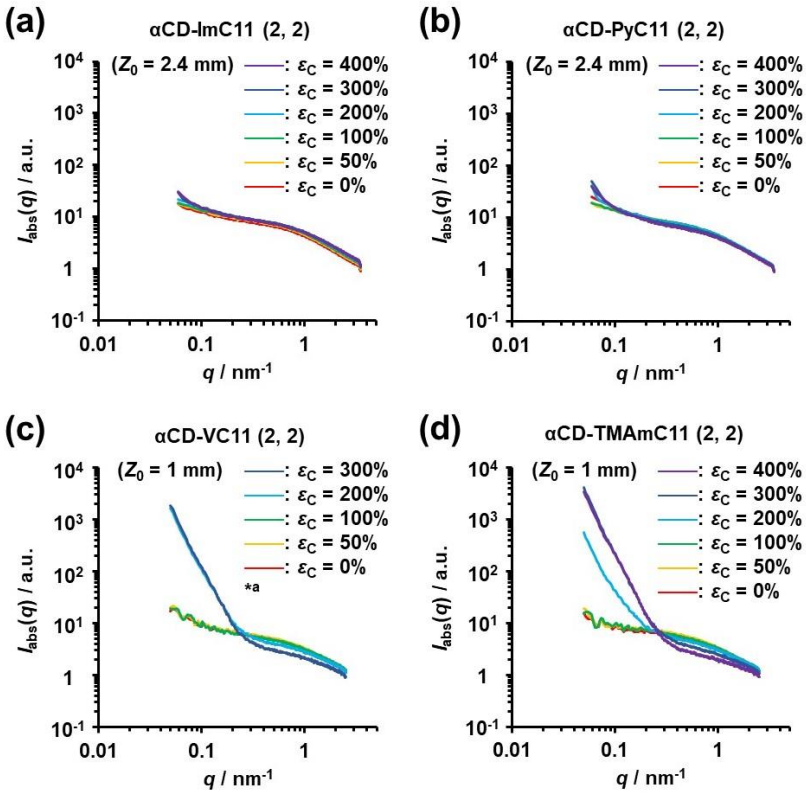

Figure S35. SAXS profiles (absolute intensity) of **(a)** αCD-ImC11 (2, 2), **(b)** αCD-PyC11 (2, 2), **(c)** αCD-VC11 (2, 2), and **(d)** αCD-TMAmC11 (2, 2) hydrogels under stretching. (Note) *[a]: The αCD-VC11 (2, 2) hydrogel broke before the strain reached 400%.

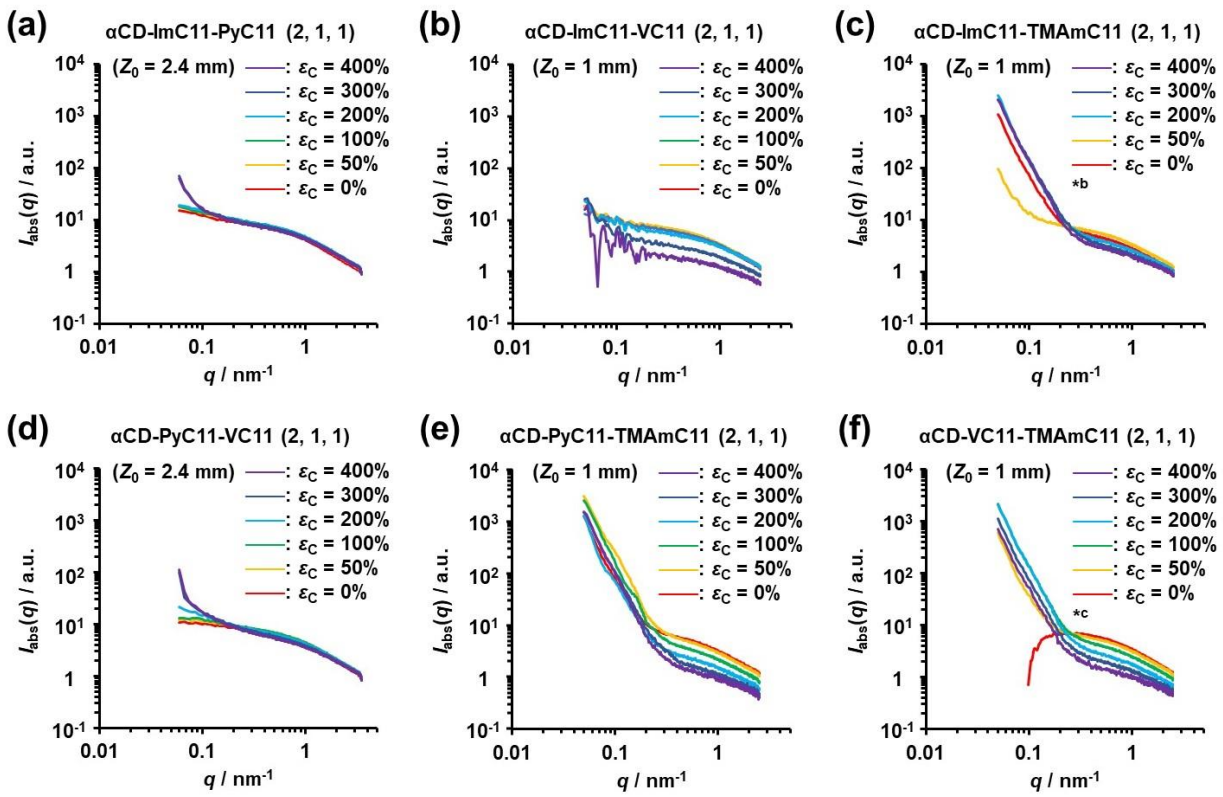

Figure S36. SAXS profiles (absolute intensity) of **(a)** αCD-ImC11-PyC11 (2, 1, 1), **(b)** αCD-ImC11-VC11 (2, 1, 1), **(c)** αCD-ImC11-TMAmC11 (2, 1, 1), **(d)** αCD-PyC11-VC11 (2, 1, 1), **(e)** αCD-PyC11-TMAmC11 (2, 1, 1), and **(f)** αCD-VC11-TMAmC11 (2, 1, 1) hydrogels under stretching. (Note) *[b]: SAXS data of the αCD-ImC11-TMAmC11 (2, 1, 1) hydrogel at a strain of 100% were not obtained due to an instrumental error. *[c]: SAXS data of the αCD-VC11-TMAmC11 (2, 1, 1) hydrogel at a strain of 0% was reduced at q < 0.2 nm^{-1} due to small difference from the background.

8. References

1 Y. Takashima, K. Otani, Y. Kobayashi, H. Aramoto, M. Nakahata, H. Yamaguchi and A. Harada, *Macromolecules*, 2018, **51**, 6318–6326.

2 Y. Takashima, Y. Sawa, K. Iwaso, M. Nakahata, H. Yamaguchi and A. Harada, *Macromolecules*, 2017, **50**, 3254–3261.

3 S. Konishi, Y. Kashiwagi, G. Watanabe, M. Osaki, T. Katashima, O. Urakawa, T. Inoue, H. Yamaguchi, A. Harada and Y. Takashima, *Polym. Chem.*, 2020, **11**, 6811–6820.

4 H. Aramoto, M. Osaki, S. Konishi, C. Ueda, Y. Kobayashi, Y. Takashima, A. Harada and H. Yamaguchi, *Chem. Sci.*, 2020, **11**, 4322–4331.